

1  
2  
3  
4  
5  
6  
7  
8  
9  
10  
11  
12  
13  
14  
15

# **Thallium concentration and thallium isotope composition of lateritic terrains**

**Howarth, S.<sup>1,2\*</sup>, Prytulak, J.<sup>1,3</sup>, Little, S. H.<sup>1</sup>, Hammond, S. J.<sup>4</sup>, Widdowson, M.<sup>5</sup>**

<sup>1</sup>Department of Earth Science and Engineering, Imperial College London, SW7 2AZ, UK

<sup>2</sup>National Oceanography Centre, School of Ocean and Earth Science, University of Southampton, SO14 3ZH, UK. S.A.Howarth@soton.ac.uk

<sup>3</sup>Department of Earth Sciences, University of Durham, DH1 3LE, UK

<sup>4</sup>School of Environment, Earth and Ecosystem Sciences, The Open University, Walton Hall, Milton Keynes, MK7 6AA, UK

<sup>5</sup>School of Environmental Science, University of Hull, Cottingham Road, Hull, HU6 7RX, UK

16 **ABSTRACT**

17 Continental weathering plays a key role in modifying the geochemical budget of  
18 terrestrial reservoirs. Laterites are the products of extreme sub-aerial continental weathering.  
19 This study presents the first investigation of thallium (Tl) abundances and stable isotopic  
20 compositions of lateritic terrains. Two laterite profiles from India of differing protolith and  
21 age are studied. Thallium concentrations range between 7 – 244 ng/g for a basalt-based  
22 lateritic profile and 37 – 652 ng/g within a greywacke lateritic profile. The average Tl stable  
23 isotope composition of the two profiles is similar to many typical igneous materials, however,  
24 the intense tropical weathering causes a small but resolvable fractionation of Tl stable  
25 isotopes towards heavy values in the residual soils. The profiles are dominated by significant  
26 positive isotope excursions (reported as  $\epsilon^{205}\text{Tl}$  relative to standard NBS997) of  $+ 3.5 \pm 0.5$   
27 2sd and  $+ 6.2 \pm 0.5$  2sd at the inferred palaeowater tables within both laterite profiles. These  
28 signatures likely reflect combined changes in redox state and mineralogy. Extensive mineral  
29 dissolution under through-flowing fluids alongside the formation of new phases such as  
30 phyllosilicates and Mn- and Fe- oxides and hydroxides likely account for some of the Tl  
31 mobilisation, sorption and coprecipitation. In the case of laterites, the formation of the new  
32 phases and role of surface sorption likely contribute to stable Tl isotope fractionation. The  
33 identification of strong isotope excursions at inferred palaeowater tables encourages future  
34 research to determine specific mineral phases that may drive significant fractionation of Tl  
35 stable isotopes. This study showcases the magnitude of natural variation possible in terrestrial  
36 soils. Such information is key to the nascent applications of Tl isotope compositions as  
37 tracers of anthropogenic pollution.

38

39 *Keywords: Laterites, Thallium Isotopes, Ferromanganese Minerals, Birnessite*

40

## 41 1. INTRODUCTION

42 The weathering of continental landmasses is one of the major modification processes  
43 operating on the surface of the Earth. It plays a significant role in the geochemical cycling of  
44 elements, from local to global scales. The effects of oxidative weathering on elemental  
45 mobility are also an important consideration for environmental impact studies. Improvements  
46 in analytical techniques in recent decades have enabled stable isotope analysis for elements  
47 spanning the periodic table (e.g., Bullen, 2012, 2014; Wiederhold, 2015; Teng et al., 2017).  
48 Such stable isotope investigations (e.g., Cr, Li, Fe, Cu, Ni) are increasingly providing insight  
49 both into continental weathering processes (e.g., Huh et al., 1998; Gall et al., 2013; Berger  
50 and Frei, 2014; Wiederhold, 2015) and the formation of laterites specifically (e.g., Kisakürek  
51 et al., 2004; Poitrasson et al., 2008; Liu et al., 2014). One element and novel isotope system  
52 whose weathering behaviour remains relatively unexplored is that of thallium (Tl).

53 The distribution and behaviour of Tl in terrestrial reservoirs is partly controlled by  
54 similarities of its relatively large ionic radius ( $Tl^+ = 1.50 \text{ \AA}$ ) to the alkali metals  $K^+$ ,  $Rb^+$  and  
55  $Cs^+$  (Shaw, 1952; Heinrichs et al., 1980). This has been used to explain the observed  
56 differences in Tl concentration between continental crust ( $\sim 0.5 \mu\text{g/g}$ ) and mantle ( $\sim 0.003$   
57  $\mu\text{g/g}$ ) (Fig. 1) due to its incompatible behaviour during mantle melting (Shaw, 1952;  
58 Heinrichs et al., 1980; Nielsen et al., 2006b; Nielsen et al., 2017a; Prytulak et al., 2017). Ionic  
59 charge is also likely to factor into the behaviour of Tl, given its existence in both monovalent  
60 and trivalent valence states (Nielsen et al., 2017a). Within low temperature environments,  
61 studies have focused largely on the most Tl-enriched reservoirs, hence the comparative  
62 wealth of work on ferromanganese (FeMn) crusts and nodules in the marine realm (e.g.  
63 Rehkämper et al., 2002; Nielsen et al., 2009, 2011, 2013; Peacock and Moon, 2012).  
64 Ferromanganese crusts have some of the highest natural Tl concentrations determined thus  
65 far, between 30 – 200  $\mu\text{g/g}$  (Fig. 1) and as such are a key reservoir in the global Tl cycle.

66 Thallium abundances within soils are comparatively low, normally ranging from 0.01 – 1  
67  $\mu\text{g/g}$  for uncontaminated soils (Kazantis, 2000; Xiao et al., 2004). Some soils have shown  
68 naturally elevated concentrations  $>5 \mu\text{g/g}$ . These tend to be associated with K-rich igneous  
69 rocks, where similar ionic radii allow for substitution of  $\text{K}^+$  or  $\text{Rb}^+$  with  $\text{Tl}^+$ , or soils  
70 occurring proximal to sulfide deposits (Xiao et al., 2004; Pavlíčková, 2006). Finally, high Tl  
71 concentrations proximal to industrial hubs has focused recent environmental research on  
72 tracking anthropogenic Tl pollution and contamination. Surface soil Tl concentrations have  
73 been shown to depend not only on substrate lithology but also on the presence of  
74 anthropogenic Tl contamination, for example from cement plants (e.g. Jacobson et al., 2005;  
75 Pavlíčková, 2006; Vaněk et al., 2009; Kersten et al., 2014; Vaněk et al., 2016; Vaněk et al.,  
76 2018). Studies of heavily contaminated soils (hundreds to thousands of  $\mu\text{g/g}$  Tl) have  
77 observed Tl associations largely with residual silicates and secondary illite-clays.  
78 Furthermore, in soils with lower Tl concentrations (few tens of  $\mu\text{g/g}$  Tl) the Tl adsorption  
79 appears dominated by Mn-oxides, with negligible adsorption onto Fe(III) oxides such as  
80 goethite (Vaněk et al., 2009; Vaněk et al., 2011; Voegelin et al., 2015; Vaněk et al, 2016).

81 Thallium stable isotope studies in low temperature environments have highlighted  
82 surprisingly large isotope fractionations. Despite the small relative mass difference between  
83 the two Tl isotopes ( $^{203}\text{Tl}$  and  $^{205}\text{Tl}$ ) of  $<1\%$ , Tl displays large natural isotope variations in  
84 excess of 35 epsilon units (corresponding to 3.5‰ in the  $\delta$ -notation, as used in other isotope  
85 systems) in low temperature environments. Isotope variations are reported relative to the  
86 NIST 997 Tl standard as  $\epsilon^{205}\text{Tl}$ , which is defined as:

$$\epsilon^{205}\text{Tl} = \left( \left( \frac{(^{205}\text{Tl}/^{203}\text{Tl})_{\text{sample}}}{(^{205}\text{Tl}/^{203}\text{Tl})_{\text{NIST 997}}} \right) - 1 \right) \times 10,000$$

87  
88 By far the largest Tl isotope fractionations have been observed within marine reservoirs  
89 and extensive work has been carried out on FeMn crusts and altered oceanic crust, which

90 display large positive and negative  $\epsilon^{205}\text{Tl}$  signatures, respectively (Fig. 1; see review in  
91 Nielsen et al. 2017a). In FeMn crusts, coupled sorption and redox effects onto specific Mn-  
92 oxides has been shown to cause Tl stable isotope fractionation (Peacock et al., 2009; Peacock  
93 and Moon, 2012; Nielsen et al., 2013). Within terrestrial environments a smaller range of  
94  $\epsilon^{205}\text{Tl}$  have been recognised. Similar Tl stable isotope values for upper continental crust and  
95 riverine detrital particulates (average  $\epsilon^{205}\text{Tl}$  of  $-2.0$  and  $-2.5$  respectively) have been used to  
96 imply negligible Tl fractionation during weathering processes, however the direct effect of  
97 weathering is yet to be studied extensively (Nielsen et al., 2005). Investigations of soils have  
98 focussed on the use of Tl stable isotope compositions as tracers of industrial processes, such  
99 as cement production and coal burning. This application relies on the existence and  
100 preservation of an ‘anthropogenic’ Tl stable isotope signature. However, the potential  
101 secondary Tl stable isotope effects from lithospheric and pedospheric processes remain  
102 poorly defined and require further investigation to better aid reliable tracing of industrial Tl  
103 emissions (Kersten et al., 2014; Voegelin et al., 2015; Vaněk et al., 2016). Potential sources  
104 of fractionation include riverine transport processes and continental weathering: the latter  
105 providing the impetus for the current study. Since lateritic profiles represent some of the most  
106 extreme enrichment and depletion behaviours that occur naturally in rock substrates as well  
107 as systematic mineralogical changes, they provide a natural laboratory to investigate Tl  
108 behaviour during weathering.

109 Here we provide the first examination of Tl and stable Tl isotope variations resulting  
110 from intensive oxidative weathering processes through the investigation of well-  
111 characterized, mature, deep weathering profiles of tropical lateritic terrains. We aim to  
112 determine the magnitude of Tl elemental and isotope variation and its most likely cause(s).  
113 Given the extent of laterites through geological time, covering  $\sim 30\%$  of continental surface  
114 area (Tardy, 1997; Dequincy et al., 2002) and with protracted formation periods,

115 understanding the behaviour of TI in extensively weathered terrains could provide important  
116 insights into the little-explored behaviour of TI in surface environments. Furthermore, our  
117 work also provides a baseline for nascent industrial anthropogenic pollution applications.

118

## 119 **2. METHODS**

### 120 *2.1. Sample Suites*

121 Two well-characterised, lateritic profiles from India of differing substrate and ages were  
122 chosen: the basaltic-based Bidar and greywacke-based Mercedes Quarry sequences  
123 (Widdowson, 2007). The spatial association of the two profiles restricts the effects of major  
124 climatic variations, and their geographic situation minimizes potential differences in exotic  
125 inputs (Fig. 2; Babechuk et al., 2015). The two profiles are extensively characterised with  
126 respect to elemental composition, mineralogy and degrees of lateritization (Mason, 1999;  
127 Widdowson and Gunnell, 1999a, 1999b; Borger and Widdowson, 2001; Kisakürek et al.,  
128 2004; Wimpenny et al., 2007; Widdowson, 2009; Babechuk et al., 2014, 2015).

129 The Bidar Profile (hereafter “BB”) is a lateritic sequence through the Deccan flood  
130 basalts, near Bidar, north-eastern Karnataka State, Central India (17°54’43” N,  
131 77°32’38”E). This 50 m deep weathering profile is capped by a thick, indurated laterite  
132 which is likely to have developed between ca. 65 – 55 Ma (Widdowson and Gunnell, 1999a,  
133 1999b) directly upon the Ambenali Formation (Fm) of the Late Cretaceous Deccan basalt  
134 succession (Widdowson, 1997; Babechuk et al., 2015). This formation is part of the Deccan  
135 Traps, a Continental Flood Basalt Province (CFBP) erupted over ~4 Ma period at 67 - 63 Ma  
136 and consisting of multiple tholeiitic flow bodies, of which the Ambenali Fm is the most  
137 extensive (Jay and Widdowson, 2008).

138 The Mercedes Quarry (hereafter “SQ”) example is a 35 m weathering profile developed  
139 upon a metagreywacke and forming part of the Panjim-Merces Plateaux in Goa, western

140 India (15°28.46' N, 73°52.33') (Widdowson, 2009). It lies within the Konkan-Kanara  
141 lowlands, and formed as an extensive belt of laterite during the mid-Neogene (Miocene) at  
142 ca. 10 – 20 Ma (Schmidt et al., 1983). The protolith is a weakly metamorphosed early  
143 Proterozoic greywacke of the Goa Group (Sanvordem Fm) of the Dharwar Supergroup. This  
144 complex comprises part of the extensive basement lithologies that underlie the Deccan CFBP  
145 and which become exposed in the south of ca. 16°N.

146 Both profiles follow the idealised laterite profile with an unaltered bedrock (i.e., protolith)  
147 at its base that is overlain by a progression into saprock, then saprolite, in which the primary  
148 texture of the rock is preserved, and then into increasingly altered zones above (Fig. 3; e.g.  
149 Martini and Chesworth, 1992; Widdowson, 2007). The saprolite zone often contains  
150 unaltered corestones within a soft saprolite matrix. Lateritization intensity increases up-  
151 profile, through the mottled zone and carapace (i.e., non-indurated levels dominated by  
152 oxyhydroxides of Fe and Al), with any remaining primary textures obscured by iron-rich  
153 segregations (i.e., mottled zone) and an increasingly open porosity eventually characterised  
154 by tubular (i.e., vermiform) textures. Both are capped by a highly indurated, resistant  
155 duricrust. The weathering of basaltic and related substrates typically involves the alteration of  
156 a mafic mineral assemblage firstly to phyllosilicates, followed by kaolinization and  
157 desilicification (Nesbitt and Young, 1989); the detail of this pattern can vary in those profiles  
158 developed on more felsic, or sedimentary protoliths (e.g. Fedo et al., 1995).

159 Here, we focus on those samples most representative of the mineralogical and textural  
160 changes within two contrasting laterite sequences, of different substrate types and ages (Fig.  
161 3; Mason, 1999; Kisakürek et al., 2004; Babechuk et al., 2014).

162 Within the SQ profile, SQ2 represents the unweathered greywacke horizon. Sample SQ1  
163 represents a small-scale mafic dyke (Widdowson, 2009). Samples SQ3 – SQ4, lie within the  
164 saprock zone. Samples SQ5 and SQ7 – SQ9, ~ above 22.5m, lie within the kaolinization field

165 and correspond to Si-depletion and Fe-enrichment, transitioning from upper saprolite and  
166 plasmic zone into the mottled zone with Fe-rich segregation. Samples SQ10 and SQ13 –  
167 SQ14 are strongly lateritized and correspond to the carapace and indurated duricrust. Samples  
168 SQ12 and above mark the progression towards secondary Fe-dominated minerals as more Si  
169 and Al is lost from the neo-formed kaolinite. Within the BB profile, samples BB1 and BB2  
170 represent the unaltered Deccan basalt and proximal saprock within Zone I that display similar  
171 chemical compositions. Samples BB3 and BB4 show mottled textures within the saprock of  
172 Zone II. BB7 and BB8 correspond to weak and moderate lateritization and the uppermost  
173 BB9 represents the indurated duricrust (Fig. 3). Extensive work carried out by Widdowson  
174 (2007) detailed the variation in major elemental composition through both the BB and SQ  
175 profiles. In both profiles, the more mobile elements (e.g. Ca, Mg, K) are lost from the  
176 saprolite zones (Zone II, Fig. 3). Above the saprolite zones an increase in Fe concentration is  
177 observed alongside a decrease in Si due to the breakdown of the protolith silicates. The small  
178 increase of SiO<sub>2</sub> in SQ6 is attributed to its proximity to a quartz vein within the profile,  
179 highlighting the greater variability in the SQ protolith. The uppermost sections of both  
180 profiles, corresponding to the iron-rich duricrust (Zone IV), show the expected enrichments  
181 in Fe<sub>2</sub>O<sub>3</sub> and corresponding depletion in SiO<sub>2</sub>. In both profiles, there are horizons that do not  
182 follow this sequence of laterite development, BB5 and BB6 in the Bidar laterite and SQ10  
183 and SQ11 in the SQ laterite (Zone III, Fig. 3). Concentrations of Fe<sub>2</sub>O<sub>3</sub> and trace elements,  
184 alongside Os and Li isotopic data, have shown that these enrichments can be attributed to the  
185 existence of palaeowater tables, which has allowed for the allochthonous input of Fe via  
186 groundwater fluxes (Kisakürek et al., 2004; Wimpenny et al., 2006).

187

## 188 *2.2. Sample Preparation*



189 The BB and SQ samples used, from the Bidar and Merces Quarry respectively, were  
190 collected by previous studies and were chosen as representative of key horizons that marked  
191 changes in mineralogy and texture (Mason, 1999; Wimpenny et al., 2007). Bulk samples of 1  
192 – 3 kg of each horizon were originally collected from multiple representative outcrops to  
193 reduce the effect of local heterogeneities within horizons (Kisakürek et al., 2004). Samples  
194 for the BB profile were powdered in a tungsten carbide mill, whereas samples for the SQ  
195 profile were prepared in an agate mill to minimize potential contamination. It should be noted  
196 that preparation in tungsten carbide versus agate is not anticipated to affect Tl concentration  
197 or isotope ratios.

198

### 199 *2.3. Major and trace elements*

200 Major element data for both the BB and SQ sequences and supplementary trace element  
201 data for the BB profile are from Babechuk et al. (2014) and Widdowson (2007). We report  
202 new high precision trace element determinations, including Tl, for both the BB and SQ  
203 sequences.

204 Trace element analysis was undertaken at the Open University, UK, with an Agilent  
205 8800 ICP-QQQ ('triple-quad' inductively coupled plasma mass spectrometer). Sample  
206 digestion was performed at the Mass Spectrometry and Geochemistry Labs at Imperial  
207 College London (MAGIC). All acids employed in chemical digestions and separations were  
208 distilled in either quartz or Teflon sub-boiling distillation systems and all Savillex Teflon was  
209 acid cleaned. De-ionized, 18 M $\Omega$ -grade water from a Millipore system-was used for rinsing  
210 and dilution. Approximately 50 mg of sample powder was dissolved in sealed Teflon vials  
211 with a 3:1 mixture of concentrated HF: HNO<sub>3</sub>. The solutions were ultra-sonicated for 25  
212 minutes and heated at 160 °C on a hot plate for at least 24 hours. They were then evaporated  
213 to near dryness and re-dissolved in 2 ml of 6 M HCl at 120 °C for at least 24 hours. The

214 solutions were then evaporated to complete dryness at 120 °C and re-dissolved in ~1 ml  
215 concentrated HNO<sub>3</sub> and evaporated at 180 °C. The last re-dissolution and evaporation step  
216 was repeated at least three times until the samples turned brownish or brown, indicating the  
217 destruction of fluorides from initial HF dissolution. Finally, an appropriate volume of 2%  
218 HNO<sub>3</sub> was added to achieve a 1000-fold sample dilution.

219 Samples were aspirated into the ICP-QQQ using a quartz microflow nebuliser, with an  
220 uptake rate of 0.5 ml per minute, and count rates in the order of  $1 - 5 \times 10^7$  cps/ppm.  
221 Analyses were performed in two different collision/reaction cell modes (no gas and He).  
222 Oxide levels (measured as CeO/Ce) were kept low, at 1% in no gas, and 0.5% in He collision  
223 mode, and doubly charged species (Ce<sup>++</sup>/Ce<sup>+</sup>) at 1.6% in no gas, and 1.2% in He collision  
224 mode. Analyses were standardized against five reference materials (digested at both the Open  
225 University and Imperial College London) that were measured at the beginning of each  
226 analytical run. The reference materials were selected on the basis of their similarity to the  
227 samples analysed, and include BIR-1, W-2, DNC-1, BHVO-2 and AGV-1. An internal  
228 standard solution (containing Be, Rh, In, Tm, Re, and Bi) was added to samples and run on-  
229 line throughout all analyses and used to correct for instrumental drift. Drift was further  
230 monitored with a measurement block consisting of USGS reference material BIR-1 (separate  
231 digest to that used in the standardization), a 2% HNO<sub>3</sub> blank, and a repeated unknown sample  
232 (SQ8) performed every five unknown measurements (see Supplementary Sheet 3). After  
233 correction for the blank values, instrumental drift and dilution weights, replicate  
234 measurement of monitoring standards yielded a precision of <2% RSD for Tl (see  
235 Supplementary Sheet 3 and Sheet 4 for trace elemental precision data). Thallium  
236 concentrations determined by ICP-MS (QQQ) are in agreement with estimated values  
237 obtained during MC-ICPMS isotope measurements (see Electronic Annex). We employ ICP-  
238 MS (QQQ) for Tl data measured in this study in all subsequent figures, due to its superior

239 precision and accuracy compared to the greater error associated with concentration  
240 determination by beam intensity matching during MC-ICPMS isotope measurements.

241

#### 242 *2.4. Determination of Tl stable isotope composition*

243 Separation of Tl from sample matrices was carried out in the MAGIC Laboratories at  
244 Imperial College London following established two-stage ion exchange chromatography  
245 protocols (Rehkämper and Halliday, 1999; Nielsen et al., 2004; Prytulak et al., 2013).

246 Thallium stable isotope compositions were determined using a Nu-Plasma HR MC-  
247 ICPMS, equipped with an ARIDUS II introduction system. Thallium fractions were diluted  
248 to concentrations between 2 and 5 ppb and doped with NIST SRM 981 Pb for a Pb/Tl ratio of  
249  $\sim 4$  in order to correct for instrumental mass fractionation. Thallium isotopes were measured  
250 using sample-standard bracketing techniques with NIST SRM 997 Tl (Rehkämper and  
251 Halliday, 1999). As the column chemistry method used provides quantitative Tl yields, with  
252 Rehkämper and Halliday (1999) confirming routine Tl elutions of  $>99.5\%$  in the applied  
253 anion-exchange procedure, Tl concentrations can be estimated to a precision of  $\sim 10\text{-}15\%$   
254 through monitoring  $^{205}\text{Tl}$  intensities using a MC-ICPMS (Rehkämper and Halliday, 1999;  
255 Nielsen et al., 2004; Nielsen et al., 2005; Prytulak et al. 2013). Multiple reference materials  
256 with known  $\epsilon^{205}\text{Tl}$  values were run for data quality control. United States Geological Survey  
257 (USGS) reference material AGV-2 and/or BCR-2 were processed and measured with every  
258 batch of unknown samples. We also present the first Tl isotope measurements of VL2, a  
259 laterite standard from Venezuela developed upon a doleritic protolith (Schorin and  
260 LaBrecque, 1983; LaBrecque and Schorin, 1987). Thallium concentrations and stable isotope  
261 composition of the samples and standards are given in Table 1 and 2. The Tl isotope  
262 composition of USGS reference materials AGV-2 and BCR-2 measured over the course of  
263 this study agree with literature values (Table 2). Repeat analyses of a Sigma Aldrich Tl

264 solution standard has shown a long-term measurement reproducibility of  $\epsilon^{205}\text{Tl} = -0.79 \pm$   
265  $0.35$  (compiled by Nielsen et al., 2017a). This study determined the Sigma Aldrich standard  
266 as  $\epsilon^{205}\text{Tl} = -0.61 \pm 0.36$  ( $n = 33$ ), in agreement with this reproducibility. Replicate digestions  
267 of most samples measured show an external 2sd reproducibility of about  $\pm 0.5 \epsilon^{205}\text{Tl}$ . A  
268 standard error of  $\pm 0.5 \epsilon^{205}\text{Tl}$  is applied to all samples except those whereby the calculated  
269 2sd between replicates exceeded this value. This includes sample BB5, with  $\epsilon^{205}\text{Tl} = +6.2 \pm$   
270  $1.5$  2sd ( $n = 4$ ), encompassing 3 separate dissolutions. Table 1 shows that there is a  
271 discrepancy between the  $\epsilon^{205}\text{Tl}$  measured for each separate dissolution, but within the second  
272 dissolution the results are self-consistent, with an average of  $\epsilon^{205}\text{Tl} = +6.2 \pm 0.7$  (2sd,  $n = 2$ ).  
273 Thus, we attribute the larger external reproducibility of this sample to powder heterogeneity,  
274 potentially generated during field sampling of this complex horizon. Total procedural blanks  
275 were  $<20$  pg Tl, negligible relative to the total processed Tl ( $>24$  ng).

276

### 277 3. RESULTS

#### 278 3.1. Thallium and other trace elements

279 Thallium concentrations and trace element determinations are shown in Tables 1 and 3.

280 The SQ profile reveals Tl concentrations ranging from 37 – 652 ng/g (Table 1, Fig. 4a),  
281 displaying an overall depletion in Tl when compared to average values for the upper  
282 continental crustal of  $\sim 750$  ng/g (Taylor and McLennan, 1985). The overall Tl concentration  
283 profile with depth in SQ is highly variable. The median concentration is 132 ng/g but the  
284 profile is dominated by high concentration spikes, with four samples exceeding the upper  
285 quartile value of 414 ng/g. Two key positive excursions in concentration occur at 22.5 m for  
286 SQ5 (652 ng/g) and 7.5 m for SQ11(544 ng/g). The lowest Tl concentration, of 37 ng/g, is at  
287 8.5 m (SQ10).

288 Concentrations of the four samples measured using ICP-QQQ for the BB profile range  
289 from 7 – 244 ng/g (Tables 1 and 2). Thallium concentrations for the full depth profile were  
290 carried out by Babechuk et al. (2014), and show a comparable range between 3 – 272 ng/g.  
291 The Bidar profile shows an increase in measured concentrations up-section, from 7 ng/g at 26  
292 m (BB3) to 39 ng/g at 5 m (BB8), with the highest concentration (244 ng/g) found at 6.0 m  
293 (BB7) (Fig. 4b).

294 The trace element concentrations within the SQ and BB profiles show similarly large  
295 variance (Table 3 and Fig. 5). Given predicted similar behaviours between Tl and elements  
296 that form species with similar ionic radii, the concentration profiles of the alkali elements can  
297 be compared. Within the SQ profile, the trace alkali elements (Cs, Li and Rb) share almost  
298 identical patterns of depletion and enrichment relative to unweathered protolith  
299 concentrations (Fig. 5a). These match the patterns of Tl through most of the profile but  
300 display markedly different behaviour for sample SQ11. Here the alkali elements do not  
301 display the extreme enrichment observed for Tl. Similarly, the trace alkaline earths (Sr and  
302 Ba) show varying concentrations relative to the Tl concentration pattern. Enrichments and  
303 depletion patterns above protolith values are well matched by Ba but Sr displays much  
304 smaller variance and depletion within all weathered samples. Within the BB profile the alkali  
305 elements also show similar patterns of enrichment and depletion relative to each other but  
306 behaviour compared to Tl deviates at BB8 and BB7 (Fig. 5b). At these horizons, the alkali  
307 elements are enriched in BB8 and depleted in BB7, which opposes the trend for Tl in both  
308 samples. For the trace alkaline earths Ba and Sr enrichments relative to the protolith are  
309 decoupled through the profile, with Ba displaying similar trends to Tl.

310

311 *3.2. Thallium stable isotope variation in laterite profiles*

312 The SQ sequence shows a large range in  $\epsilon^{205}\text{Tl}$  from  $-2.4$  to  $+3.5$ , which is variable  
313 throughout the profile but generally shows a slight increase in  $\epsilon^{205}\text{Tl}$  up-profile, with the  
314 exception of a prominent positive excursion of  $\epsilon^{205}\text{Tl} = +3.5$  at SQ11 (Fig. 4b).

315 The lightest  $\epsilon^{205}\text{Tl}$  value occurs at 25.5 m for SQ4 and the heaviest occurs at 7.5 m for  
316 SQ11 (Fig. 4b). There is a slight general increase in The BB sequence  $\epsilon^{205}\text{Tl}$  values range  
317 from  $-0.5$  to  $+6.2$ . The lightest  $\epsilon^{205}\text{Tl}$  is BB8 at 5 m (Fig. 4b). Trends within the profile are  
318 less well defined due to fewer data points, but at 13 m the outlying and distinctive feature is  
319 an excursive heavy  $\epsilon^{205}\text{Tl} = +6.2$  for BB5. The profile average for all samples analysed is  
320  $\epsilon^{205}\text{Tl} = +2.0 \pm 3.7$  (1sd,  $n = 3$ ). Low Tl concentrations (e.g., BB1  $\sim 3$  ppb; Babechuk et al.,  
321 2014) require in excess of 1 g of sample for repeat Tl isotopic measurement, of which there  
322 was insufficient characterised material remaining. However, unweathered basalt is assumed  
323 to have Tl content comparable to mid-ocean ridge basalts (MORBs) (Nielsen et al., 2006a),  
324 hence a value of  $\epsilon^{205}\text{Tl} \sim -2.0 \pm 1$  is assumed for the protolith (BB1) (e.g. Fig 4). When this  
325 assumed value of  $\epsilon^{205}\text{Tl}$  is used to approximate BB1 the average for the profile is  $\epsilon^{205}\text{Tl} = +$   
326  $1.0 \pm 7.2$  (2sd,  $n = 4$ ). For the BB sequence a correlation between Tl concentrations and  
327  $\epsilon^{205}\text{Tl}$  cannot confidently be drawn due to the small dataset but the excursive nature of BB5 is  
328 clear (Fig. 6). The VL2 laterite standard measured shows a heavy  $\epsilon^{205}\text{Tl} = +2.1 \pm 0.5$  which  
329 is closely matched to the average Tl isotopic composition of the BB profile.

330

#### 331 4. DISCUSSION

332 Both the basaltic BB and greywacke-based SQ sequences show variable depth profiles  
333 with respect to both Tl concentrations and stable isotope signatures (Fig. 4a and 4b). *A priori*  
334 these variations could be considered the result of two natural factors. Firstly, processes  
335 internal to the laterite profile, which could drive redistribution of Tl and/or significant stable  
336 isotope fractionation. Secondly, external fluxes of Tl to and from the laterite profiles.

337 In order to quantify the overall addition and loss of elements in weathering profiles,  
338 relative to the unaltered protolith levels, we calculate the  $\tau$ -parameter following Chadwick et  
339 al. (1990). The  $\tau$ -parameter describes the proportion of a selected element gained or lost at a  
340 chosen horizon within a weathering profile, relative to an immobile index element. The least  
341 mobile element identified for both profiles was Zr, because it displays the smallest variation  
342 relative to protolith concentrations (Widdowson and Cox, 1996). The  $\tau$ -parameter is  
343 calculated as follows:

$$344 \quad \tau_{i/Zr} = \left[ \frac{(C_i/C_{Zr})_h}{(C_i/C_{Zr})_p} \right] - 1$$

345 where C is the concentration, h represents the horizon of interest and p represents the  
346 unaltered protolith values (samples BB1 and SQ2).  $\tau$ -values are shown in Table 4. Values  $> 0$   
347 indicate enrichment of element of interest  $i$  and values  $< 0$  indicate loss of  $i$  relative to the  
348 unweathered substrate. When summed throughout the profile the total  $\tau$ -value can give an  
349 indication of net gain or loss of element  $i$  to the profile versus internal mobilization and  
350 vertical transport.

351 The extent of weathering through the profiles also needs to be quantified in order to  
352 investigate the role of weathering and chemical alteration on Tl concentration and stable  
353 isotope systematics. The most commonly applied indices of chemical alteration used are the  
354 Chemical Index of Alteration (CIA) and the Mafic Index of Alteration (MIA). Both employ  
355 bulk major elemental molar ratios but do not include the proportion of SiO<sub>2</sub> in their  
356 calculations and insufficiently capture the more extreme, late-stage weathering and  
357 desilicification processes which occur during lateritization (Babechuk et al., 2014). In this  
358 study, the Index of Lateritization (IOL) method was chosen following extensive work  
359 characterizing degrees of alteration through BB and SQ profiles (Table 4, Widdowson et al.,  
360 2007, 2009; Babechuk et al. 2014). These studies analysed samples from both sequences

361 using methods developed by Schellman (1986), based on  $\text{SiO}_2\text{-Al}_2\text{O}_3\text{-Fe}_2\text{O}_3$  tri-plots.  
362 Regions on the ternary diagram are separated into degrees of alteration, ranging from  
363 unaltered protolith values, through the “limit of kaolinization” and then defining weak,  
364 moderate and strong lateritization (Widdowson, 2009). The limits of kaolinization occur at  
365 ~43 wt%  $\text{SiO}_2$  for BB and at ~57 wt%  $\text{SiO}_2$  and a common lateritization process is proposed  
366 across western India (Widdowson, 2007, 2009; Wimpenny, 2007; Babechuk et al., 2014). For  
367 both profiles, the IOL is shown to be representative of general trends in degree of  
368 lateritization (when accounting for environmental conditions) and so the following equation  
369 is applied:

$$370 \quad \text{Index of Lateritisation (IOL)} = 100 \times \frac{\text{Al}_2\text{O}_3 + \text{Fe}_2\text{O}_3}{\text{SiO}_2 + \text{Al}_2\text{O}_3 + \text{Fe}_2\text{O}_3}$$

371 Two general features are observed in the profiles of Tl and  $\epsilon^{205}\text{Tl}$  variation with depth  
372 (Fig. 4b and Fig. 6). Firstly, there is a general upsection trend in each profile. In the case of  
373 the SQ profile, the upsection Tl concentrations become increasingly depleted with respect to  
374 the protolith when normalised to Zr and  $\epsilon^{205}\text{Tl}$  become more positive. The BB profile  
375 displays different behaviour upsection, with generally increasing concentrations of Tl  
376 associated with a shift towards heavy  $\epsilon^{205}\text{Tl}$ , however, this sample set is much more limited.

377 Secondly, the most distinctive feature of both profiles is the significant Tl enrichment  
378 at specific horizons, at 6 m in the BB profile (BB7) and 7.5 m in the SQ profile (SQ11) (Fig.  
379 6). Due to the differences in magnitude and direction of the two features it is likely that two  
380 distinct processes are responsible, and they are thus discussed separately in the following  
381 sections (see Sections 4.1 and 4.2).

382

#### 383 *4.1. Behaviour of Tl and isotope fractionation of Tl during in-situ lateritic weathering*

384 Firstly, the role of in-situ weathering on Tl and Tl stable isotopes can be examined  
385 through comparing the IOL with Tl concentration and  $\epsilon^{205}\text{Tl}$  (Fig. 8 and Fig. 9), excluding the



386 heavy  $\epsilon^{205}\text{Tl}$  samples (SQ11 and BB5) which will be discussed in section 4.2. For Tl  
387 behaviour in the SQ profile, weak negative correlations are observed between Tl  
388 concentration and  $\epsilon^{205}\text{Tl}$  ( $R^2 = 36\%$ ). This correlation is stronger between  $\tau_{\text{Tl/Zr}}$  and  $\epsilon^{205}\text{Tl}$   
389 (Fig. 10;  $R^2 = 57\%$ ). This could imply that a vertical mixing mechanism could be partly  
390 responsible for the range of  $\epsilon^{205}\text{Tl}$  observed, between a higher concentration end-member  
391 with  $\epsilon^{205}\text{Tl} \sim < -2.0$  and a lower concentration, heavier reservoir with  $\epsilon^{205}\text{Tl} \sim 0$ . This  
392 vertical redistribution is possible within the SQ profile where most of the weathered samples  
393 overlying the greywacke protolith (SQ2) show Tl depletions relative to the protolith (Fig. 4a)  
394 and maybe be significant in Zone I (Fig. 10). To investigate whether the driver for this  
395 redistribution is weathering intensity, the Tl profile is compared to IOL (Fig. 8). The limit of  
396 kaolinization for the SQ profile occurs at  $\sim 57\%$   $\text{SiO}_2$ , below which desilicification starts and  
397 the extent of lateritization can be classified by increasing intensity. Slight variance in the  
398 metagreywacke protolith will also affect starting Fe- and Si- content, with protolith  
399 compositions ranging between  $\sim 15 - 25\%$   $\text{SiO}_2$ . There is a strong positive correlation ( $R^2 =$   
400  $98\%$ ) between an increase in IOL with Tl concentration for samples with  $\text{IOL} < \sim 25$ , before  
401 substantial desilicification and Fe- enrichment occur. Above this limit, for kaolinized and  
402 lateritized samples, any linear correlation ceases. This shift into kaolinization and  
403 lateritization coincides with the breakdown of primary mineralogy (largely silicates) and the  
404 formation of neo-clays and Fe- and Al-enrichment secondary phases (Widdowson, 2009). We  
405 propose that the distinct shift in the Tl concentration-IOL relationship at this horizon reflects  
406 mineralogical changes. Breakdown of primary mineralogy above  $\sim 20\text{m}$  likely allows for the  
407 remobilization and transportation of Tl vertically, for example concentrating at  $22.5\text{m}$  (SQ5,  
408  $652\text{ ng/n Tl}$ ), or for removal of Tl laterally by groundwaters. Overall the  $\tau_{\text{Tl/Zr}}$  values for the  
409 SQ profile indicate an overall loss of Tl from the profile.

410           Within the BB profile the relationship between Tl mobility and degree of lateritization  
411 is much less distinct. The  $\tau_{\text{Tl/Zr}}$  values from this profile show that there has been significant  
412 enrichment of Tl above protolith values and an overall addition of Tl. External inputs of Tl  
413 likely play a considerable role in the Tl concentration pattern for this profile and potential  
414 sources are discussed in Section 4.2.

415           In order to investigate Tl and Tl isotope behaviour during further lateritization and  
416 associated mineralogical changes, it is useful to compare its concentration profile and  
417 mobility with other major and trace elements.

418           Through the SQ profile, when water table sample SQ11 is not considered, very strong  
419 correlations ( $R^2 > 80\%$ ) are observed for Zr-normalised concentrations of Rb (99%), Li (97  
420 %), Cs (96%), Co (96%) and Zn (95%). This is matched by very strong major element  
421 correlations with MgO and K<sub>2</sub>O. When sample SQ11 is included, Tl concentrations in the full  
422 SQ profile shows strong correlations ( $R^2 > 80\%$ ) for Zn (96%), Ba (87%), Lu (85%) and  
423 Co (83%). Within the BB profile, when including supplementary trace element data, strong  
424 correlations are only observed for Ba (95%) and Pb (85%). These correlations in BB are  
425 maintained when palaeowater table horizons are removed from the analysis. When the  
426 mobility of elements ( $\tau_{i/\text{Zr}}$ ) is considered rather than normalised concentration,  $\tau_{\text{Tl/Zr}}$  shows  
427 positive correlation with  $\tau_{\text{Ba/Zr}}$  (87%) in SQ and  $\tau_{\text{Ba/Zr}}$  (88%) and  $\tau_{\text{Pb/Zr}}$  (87%) in BB. This  
428 suggests that when considering in-situ weathering processes alone, Tl behaviour is largely  
429 comparable to that of the alkali metals which share similarly large ionic radii (Shaw, 1952;  
430 Heinrichs et al., 1980; Babechuk et al., 2014; Nielsen et al., 2017a). The major host of these  
431 elements in primary minerals include a large suite of K-bearing minerals, particularly micas  
432 and feldspars (Prinz, 1967; Heinrichs et al., 1980). During weathering and lateritization the  
433 breakdown of these minerals commonly forms secondary clays, such as smectites. The alkali  
434 earths are commonly associated with these clays as they can adsorb onto the mineral surfaces

435 or substitute into interlayer sites. Studies of other laterite complexes have observed the  
436 preferential retention of Ba on clay minerals when compared with the other alkaline earths  
437 and alkali metals (e.g. Nesbitt et al., 1980; Das and Krishnaswami, 2007; Buggle et al.,  
438 2011). Furthermore, Ba can also be retained by secondary Fe- and Mn-oxides (e.g. Das and  
439 Krishnaswami, 2007; Bonnet et al., 2014). In both profiles the uppermost sections of the  
440 laterite, the duricrust and indurated cap, represent the development of secondary Fe-minerals  
441 dominated horizons, though the highest Fe-enrichments are observed near the inferred  
442 palaeowater tables.

443         Thallium stable isotopes also show IOL-dependent behaviour (Fig. 9). Below 12 m  
444 depth, where samples are unaltered to weakly lateritized, a weak positive correlation ( $R^2 =$   
445 56%) is observed between the degree of lateritization and  $\epsilon^{205}\text{Tl}$  (Zones I and II: Fig. 9). This  
446 general trend could be driven by the preferential removal of isotopically-light  $^{203}\text{Tl}$  during the  
447 early stages of kaolinization. Above this depth samples are strongly lateritized, with IOL  
448 ranging from 80 – 86, and display relatively static  $\epsilon^{205}\text{Tl}$  values of – 1.2 to – 1.0, with the  
449 exception of palaeowater table samples discussed in Section 4.2. This could imply that a  
450 threshold in the preferential mobilization of  $^{203}\text{Tl}$  is reached during the stages of intense  
451 lateritization. This threshold in preferential removal of  $^{203}\text{Tl}$  is supported by comparable  
452 trends in the relationship between  $\epsilon^{205}\text{Tl}$  and  $\tau_{\text{Tl/Zr}}$  (Fig. 10), which show a weak correlation  
453 between loss of Tl and increasingly heavy Tl isotope composition. When  $\epsilon^{205}\text{Tl}$  is compared  
454 to Zr-normalised elemental concentrations, no strong correlations with any of the measured  
455 elements are observed in SQ. Furthermore, while weathering can account for the isotopic  
456 variations of  $\epsilon^{205}\text{Tl} = -2.2$  to  $+0.3$  observed through the section, this process cannot  
457 adequately explain the significant and common excursive nature of both the horizons  
458 proximal to the water tables.

459

460       4.2. *Tl-enriched and heavy  $\epsilon^{205}\text{Tl}$  horizons*

461       Overall, variations in Tl concentrations interrogated using  $\tau$ -values show a net enrichment  
462 of Tl in the basaltic BB profile and a net loss from the greywacke-based SQ profile (Table 4).  
463 All four measured horizons in the basaltic laterite show evidence for an external source of Tl,  
464 with Tl concentrations exceeding protolith levels (Fig. 7b). For the greywacke-based SQ  
465 profile all samples except SQ5 and SQ11 indicate a loss of Tl relative to the protolith  
466 concentration of SQ2. The high Tl concentration of the unaltered SQ protolith means that  
467 there would be sufficient Tl within the SQ profile that the concentration pattern observed  
468 with depth could theoretically be explained using a simple model closed-system  
469 redistribution of Tl. The relationship between degree of lateritization and Tl mobility in SQ  
470 challenges this theory, however. A distinct shift in IOL in the SQ profile is observed between  
471 12 m – 8.5 m depth (Table 4), which is recognized by Widdowson (2007) as the transition  
472 between the kaolinized zone below and the strongly lateritized region above. If weathering  
473 were the main process driving Tl concentration variations, we would expect to observe a  
474 strong correlation between weathering intensity (IOL) and Tl mobility ( $\tau_{\text{Tl/Zr}}$ ) (Fig. 11). The  
475 absence of any systematic relationship between the two therefore supports the addition of  
476 allochthonous Tl is also likely to the SQ profile too.

477

478       4.2.1. *Aeolian Tl fluxes to laterites*

479       Numerous studies investigating elemental mobility within the BB profile show  
480 geochemical evidence for significant aeolian dust influxes, supported by  $^{87}\text{Sr}/^{86}\text{Sr}$ ,  
481  $^{143}\text{Nd}/^{144}\text{Nd}$ , Li-isotopes, Re/Os ratios and high field strength element systematics  
482 (Mason, 1999; Kisakürek et al., 2004; Wimpenny et al., 2007; Babechuk, 2015). Wimpenny et  
483 al. reported that Re/Os ratios of lateritized samples in SQ were sufficiently less radiogenic  
484 than parent values, also suggesting that external inputs were likely significant. It was

485 postulated that the most likely dust source region for both sequences would be from the  
486 surrounding Dharwar Craton, a complex of Archean to Proterozoic greywackes, mafic to  
487 ultramafics and metabasic rocks (Klootwijk and Peirce, 1979; Devaraju et al., 2010). While  
488 variations in Tl concentration are likely affected by external inputs to the profile, the  
489 attribution of the heavy  $\epsilon^{205}\text{Tl}$  excursions in both of the BB and SQ profiles to influxes of  
490 allochthonous aeolian Tl requires a source reservoir of heavy  $\epsilon^{205}\text{Tl}$ . However, the  
491 geographical locations and differing ages of the laterite profiles does not support the input of  
492 exotic materials with very different  $\epsilon^{205}\text{Tl}$  values over a  $\sim 40$  Myr time period. The basaltic  
493 BB sequence lies within the laterally extensive and geochemically uniform Ambenali Fm  
494 (Widdowson and Gunnell, 1999a, 1999b) and the SQ sequence lies within the Dharwar  
495 Supergroup of metamorphosed greywackes. Aside from the distinct heavy horizons recorded  
496 in this study, no other isotopically heavy terrestrial reservoirs of Tl have been reported.  
497 Investigations into the Tl isotope characteristics of terrestrial reservoirs have shown relatively  
498 uniform averages for loess and river particles, and hence continental crust, of  $\epsilon^{205}\text{Tl} = -2.0 \pm$   
499  $0.5$  (Nielsen et al., 2005; Nielsen et al., 2006a; Nielsen et al., 2006b). Furthermore, Os  
500 isotope studies indicate that aeolian fluxes alone cannot account for the total influx budget of  
501 Os, so the potential role of cosmic dust was suggested (Wimpenny et al., 2007). Since the  
502 formation of both the BB and SQ laterites it was estimated that cosmic dust could account for  
503  $<1\%$  of the total Os content observed in each profile. Given comparable concentrations of Tl  
504 and Os in both cosmic dust ( $\sim 50$  ng/g) and the laterite profiles (Ander and Grevasse, 1989;  
505 Wimpenny et al., 2007; Baker et al., 2010), it follows that the cosmic dust flux of Tl to  
506 laterites is unlikely to explain the large Tl enrichments above unweathered substrate  
507 concentrations observed in BB and SQ.

508 Overall these observations suggest that Tl concentrations within the profile have  
509 likely been affected by the influx of aeolian material, particularly within the BB laterite. In

510 contrast, the large variations in the  $\epsilon^{205}\text{Tl}$  profile are unlikely to be solely driven by aeolian  
511 inputs. We suggest that the Tl isotope systematics within the laterites are likely further  
512 influenced by groundwaters.

513

#### 514 4.2.2. *The role of the palaeowater table*

515 Comparable Tl stable isotope fractionations are observed proximal to the inferred  
516 palaeowater table in both laterite sequences of differing substrate age and lithology, age of  
517 lateritization, and location (Fig. 4b). This striking similarity between two very different  
518 laterite profiles implies a common process or environment as a driver of Tl stable isotope  
519 fractionation. Both laterite profiles in this study contain a high abundance of Fe  
520 oxides/oxyhydroxides (Table 1, and Fig. 3), particularly hematite and goethite, as well as  
521 clays such as kaolinite in the upper sections (Wimpenny et al., 2007). This mineral  
522 assemblage is common to many laterites of similar substrates (e.g. Ma et al., 2007;  
523 Widdowson, 2007; Fernández-Caliani and Cantano, 2010). Whilst these minerals are  
524 abundant across large sections of the profiles, over a thickness of approximately 10 m, the  
525 heavy  $\epsilon^{205}\text{Tl}$  excursions occur in discrete horizons,  $\leq 5$  m thick (Table 1 and Fig. 4b). Several  
526 studies have highlighted elemental enrichment patterns and isotopic excursions that support  
527 the existence of a palaeowater table (Mason, 1999; Kısakürek et al., 2004; Wimpenny et al.,  
528 2006; Widdowson, 2007). This horizon and capillary zones coincide with samples SQ10 and  
529 SQ11 and BB5 and BB6. Water tables within laterites form boundary horizons, below which  
530 conditions are generally suboxic and above which conditions are oxic and susceptible to the  
531 influx of oxic rainwater (e.g. Wimpenny et al., 2007). Open-system conditions allow for the  
532 lateral movement and transport of ions in solution and play a key role in the alteration  
533 minerals formed. For example, reduced conditions allow for the reduction of Fe(III) to  
534 soluble Fe(II) species below the palaeowater table, whereas the transition to oxic conditions

535 above the water table can oxidise Fe(II) to Fe(III) and trigger Fe-oxide precipitation  
536 (Kisakürek et al., 2004). These palaeowater tables can therefore superimpose further  
537 mineralogical and elemental alteration on weathering profiles, in addition to providing an  
538 allochthonous flux.

539         Within the SQ and BB profiles, correlations in elemental behaviour have highlighted  
540 the likely importance of primary and secondary mineralogy during weathering on Tl  
541 concentration. For both profiles, the strong correlation between Tl and Ba in particular  
542 appears unaffected by changes in conditions at the palaeowater tables (Fig. 5). In surface  
543 weathering environments two main phases are important in the cycling of Ba; Fe- and Mn-  
544 oxides and phyllosilicates. Few detailed studies have been carried out on mineral-specific  
545 fractionation for Tl stable isotopes. The largest isotopic fractionations for heavy element  
546 systems like Tl have been predicted where nuclear field shift effects occur (Bigeleisen, 1996;  
547 Schauble, 2007). Both the nuclear field shift effect and mass-dependent fractionation enrich  
548 the more oxidized Tl(III) species in the heavier  $^{205}\text{Tl}$  isotope, when Tl(III) is in equilibrium  
549 with reduced Tl(I) (Schauble, 2007). Under the conditions of most surface environments  
550 Tl(I) dominates as the more thermodynamically stable species (Law and Turner, 2011). One  
551 environment where Tl(III) has been both predicted and observed is at the mineral surfaces of  
552 specific Mn-oxides (Peacock and Moon, 2012; Nielsen et al., 2013). There is widespread  
553 evidence of the preferential association of Tl with Mn-oxides in both terrestrial and marine  
554 reservoirs, through Tl substitution with K and adsorption-oxidation reactions (e.g.  
555 Rehkämper and Nielsen, 2004; Vaněk et al., 2011; Kersten et al., 2014). Hydrogenetic FeMn  
556 crusts display large positive  $\epsilon^{205}\text{Tl}$  values of up to  $\sim +14$  epsilon units (Rehkämper et al.,  
557 2002; Nielsen et al. 2017a), similar to those observed in this study within the terrestrial  
558 realm. Peacock and Moon (2012) attribute the FeMn crust Tl isotope signature to the  
559 adsorption and oxidation of Tl(I) to Tl(III) during inner-sphere complexation onto hexagonal

560 birnessite (Hx-birnessite). Thallium isotope fractionation is not observed within the limited  
561 other Mn-oxides which have been measured, including todorokite and vernadite (e.g.  
562 Peacock and Moon, 2012). Other mineral species are known to be important host phases  
563 within soil complexes. For example, Tl(I) uptake by illite-type clays has been observed, with  
564 Tl substituting for K in illite (e.g. Voegelin et al., 2015). Further focused studies on potential  
565 mineral-specific fractionation effects are required to investigate whether interaction with  
566 illite-type clays can cause significant fractionation of Tl stable isotopes.

567 The strikingly heavy  $\epsilon^{205}\text{Tl}$  signals at the paleo water table horizons are of the same  
568 magnitude and direction as the Tl isotope fractionations observed in the FeMn crusts,  
569 attributed to Hx-birnessite (Peacock and Moon, 2012). In particular, within the SQ profile  
570 this heavy  $\epsilon^{205}\text{Tl}$  excursion coincides with peaks in Tl, Mn and  $\text{Fe}_2\text{O}_3$  content. Furthermore,  
571 the shift to higher  $\text{Fe}_2\text{O}_3$  begins just below the Tl peak, within sample SQ10, whereas the  
572 peak in Tl and Mn concentration coincide distinctly within SQ11. Therefore, we suggest that  
573 the  $\epsilon^{205}\text{Tl}$  variation within the SQ laterite may reflect changing Mn-mineralogy. Through the  
574 majority of the profile the presence of todorokite or similar Mn-oxides, which are not  
575 associated with a Tl isotope fractionation, could occur via the transformation of birnessite. At  
576 the palaeowater tables, oxidative conditions could thus inhibit the transformation of birnessite  
577 to todorokite. Higher oxidation states have been proposed to alter the structure of birnessite,  
578 impeding the initiation of the first step in the four-stage birnessite to todorokite  
579 transformation (Cui et al., 2008; Cui et al., 2009).

580 Within the BB profile the heaviest  $\epsilon^{205}\text{Tl}$  horizon coincides with the highest  $\text{Fe}_2\text{O}_3$   
581 content but peaks in Tl and Mn concentration occur 2m higher in the profile. This may  
582 suggest that Mn-oxide mineralogy may not be the dominant control on Tl behaviour in this  
583 profile. Thus, whilst we speculate that the positive Tl isotope excursions at the palaeowater  
584 tables are due to the presence of birnessite instead of todorokite, the Tl concentrations within



585 the laterite sequences are insufficient to quantitatively determine the diagnostic 7 and 10 Å  
586 spacings using X-ray absorption spectroscopy (Peacock and Moon, 2012). Thallium  
587 fractionation at comparable concentrations has been investigated using sequential extraction  
588 methods (e.g. Vaněk et al., 2009; Vaněk et al., 2011). Given the magnitude of natural  
589 variations observed in the laterite profiles, exploration of the specific mineral phase(s)  
590 associated with Tl isotope fractionation is a fruitful avenue for future research.

591

## 592 **5. CONCLUSIONS**

593 This study provides the first characterization of Tl concentrations and stable isotope  
594 compositions within lateritic weathering profiles. Thallium concentrations range between 7 –  
595 244 ng/g for the Bidar basaltic-based profile and 37 – 652 ng/g for the Goan greywacke-  
596 based profile. Considerable variation in Tl stable isotope ratios were observed, from – 2.4 to  
597 + 6.2. In particular, distinct heavy  $\epsilon^{205}\text{Tl}$  excursions at or near palaeowater table horizons  
598 highlight the need to characterize the Tl isotope systematics of surface reservoirs to improve  
599 our understanding of Tl cycling in surface environments. In addition, there is a small (~1 – 2  
600 epsilon units) but discernible effect of continental weathering on Tl isotopes. Thus, both  
601 weathering and horizons of enhanced fluid circulation such as paleo-water tables are likely to  
602 impact primary  $\epsilon^{205}\text{Tl}$  values, for example from industrial pollution processes (Kersten et al.,  
603 2014). Further characterization of natural surface processes and other potential  
604 mineralogically driven mechanisms of Tl stable isotope fractionation is required before the  
605 effects of anthropogenically driven-Tl isotope variations can be fully assessed.

606 The processes that occur at the palaeowater table of weathering profiles are complex,  
607 with numerous documented excursions in elemental concentrations and isotopic values. This  
608 regime has a significant effect upon the availability and flux of the elements to the wider  
609 groundwater and associated fluvial systems. The BB profile highlights the importance of

610 external fluxes of Tl to weathering profiles developed on low-Tl substrates. There is also  
611 strong evidence for the role of groundwater in the redistribution of redox sensitive elements  
612 and the formation of alteration minerals. These processes have resulted in fractionations of ~  
613 + 6  $\epsilon^{205}\text{Tl}$  from the profile averages proximal to the palaeowater table, regardless of location,  
614 lithology, age and timing of lateritization. A mechanism of mineralogically driven Tl isotope  
615 fractionation, similar to that of Mn-oxides in marine FeMn crusts (Peacock and Moon, 2012)  
616 could result in heavy  $\epsilon^{205}\text{Tl}$  signatures at redox boundaries, such as the palaeowater table  
617 horizon in the SQ profile. To improve the understanding of Tl and Tl stable isotope  
618 behaviour in surface environments, further work is required to characterize the mineral-  
619 specific behaviour of Tl.

620

## 621 Acknowledgements

622 We thank three anonymous reviewers and editorial handling by Jan Wiederhold for helpful  
623 comments that significantly improved prior versions of this manuscript. This work formed  
624 the basis of SH's final year undergraduate thesis at Imperial College London. Barry Coles  
625 and Katharina Kressig are gratefully acknowledged for their efforts in keeping the mass  
626 spectrometers and clean labs functioning, respectively. Sophie Munson is thanked for her  
627 help with trace element digestions. SHL acknowledges support from the Leverhulme Trust  
628 and a NERC independent research fellowship.

629

## 630 6. REFERENCES

- 631 Anders E. and Grevesse N., (1989) Abundances of the elements: meteoritic and solar.  
632 *Geochimica et Cosmochimica Acta*, **53**, 197–214.  
633 Babechuk M. G., Widdowson M. and Kamber B. S. (2014) Quantifying chemical weathering  
634 intensity and trace element release from two contrasting basalt profiles, Deccan Traps,  
635 India. *Chemical Geology*, **363**, 56–75.

- 636 Babechuk M. G., Widdowson M., Murphy M. and Kamber B. S. (2015) A combined Y/Ho,  
637 high field strength element (HFSE) and Nd isotope perspective on basalt weathering,  
638 Deccan Traps, India. *Chemical Geology*, **396**, 25–41.
- 639 Baker R. G. A., Rehkämper M., Ihlenfeld C., Oates C. J., Coggon R. M. (2010) Thallium  
640 isotope variations in an ore-bearing continental igneous setting: Collahuasi formation,  
641 Northern Chile. *Geochimica et Cosmochimica Acta*, **74**, 4405–4416.
- 642 Berger A. and Frei R. (2014) The fate of chromium during tropical weathering: A laterite  
643 profile from Central Madagascar. *Geoderma*, **213**, 521–532.
- 644 Bigeleisen J. (1996) Temperature dependence of the isotope chemistry of the heavy elements.  
645 *Proceedings of the National Academy of Sciences*, **93**, 9393–9396.
- 646 Bonnet N. J., Beauvais A., Arnaud N., Chardon D., and Jayananda M. (2014) First  
647  $^{40}\text{Ar}/^{39}\text{Ar}$  dating of intense Late Palaeogene lateritic weathering in Peninsular India.  
648 *Earth and Planetary Science Letters*, **386**, 126–137.
- 649 Borger H. and Widdowson M. (2001) Indian laterites, and lateritic residues of southern  
650 Germany: a petrographic, mineralogical, and geochemical comparison. *Zeitschrift für*  
651 *Geomorphologie*, **45**, 177–200.
- 652 Buggle B., Glaser B., Hambach U., Gerasimenko N., and Markovič S. (2011) An evaluation  
653 of geochemical weathering indices in loess-paleosol studies. *Quaternary International*,  
654 **240**, 12–21.
- 655 Bullen T.D. (2012) Stable Isotopes of Transition and Post-Transition Metals as Tracers in  
656 Environmental Studies. In *Handbook of Environmental Isotope Geochemistry*.  
657 *Advances in Isotope Geochemistry* (ed. Baskaran M.). Springer, Berlin, Heidelberg
- 658 Chadwick O. A., Brimhall G. H., and Hendricks D. M., (1990) From a black to a gray box -  
659 mass balance interpretation during pedogenesis. *Geomorphology*, **3**, 369 – 390.
- 660 Cui H., Liu X., Tan W., Feng X., Liu F., and Ruan H. D. (2008) Influence of Mn (III)  
661 availability on the phase transformation from layered buserite to tunnel-structured  
662 todorokite. *Clays and Clay Minerals*, **56**, 397–403.
- 663 Cui H., Qiu G., Feng X., Tan W., and Liu F. (2009) Birnessites with different average  
664 manganese oxidation states synthesized, characterized, and transformed to todorokite at  
665 atmospheric pressure. *Clays and Clay Minerals*, **57**, 715–724.
- 666 Dequincey O., Chabaux F., Clauer N., Sigmarsson O., Liewig N., and Leprun J. C. (2002)  
667 Chemical mobilizations in laterites: Evidence from trace elements and  $^{238}\text{U}$ - $^{234}\text{U}$ - $^{230}\text{Th}$   
668 disequilibria. *Geochimica et Cosmochimica Acta*, **66**, 1197–1210.
- 669 Das, A. and Krishnaswami, S. (2007). Elemental geochemistry of river sediments from the  
670 Deccan Traps, India: Implications to sources of elements and their mobility during  
671 basalt-water interaction. *Chemical Geology*, **242**, 232–254.
- 672 Devaraju T. C., Sudhakara T. L., Kaukonen R. J., Viljoen R. P., Alapieti T. T., Ahmed S. A.,  
673 and Sivakumar S. (2010). Petrology and geochemistry of greywackes from Goa-  
674 Dharwar sector, western Dharwar craton: Implications for volcanoclastic origin.  
675 *Journal of the Geological Society of India*, **75**, 465–487.
- 676 Fedo C. M., Nesbitt H. W. and Young G. M. (1995) Unravelling the effects of potassium-  
677 metasomatism in sedimentary rocks and paleosols, with implications for weathering  
678 conditions and provenance. *Geology*, **23**, 921–924.
- 679 Fernández-Caliani J. C. and Cantano M. (2010) Intensive kaolinization during a lateritic  
680 weathering event in South-West Spain; Mineralogical and geochemical inferences from  
681 a relict paleosol. *Catena*, **80**, 23–33.
- 682 Gall L., Williams H. M., Siebert C., Halliday A.N., Herrington R.J. and Hein J.R. (2013)  
683 Nickel isotopic compositions of ferromanganese crusts and the constancy of deep ocean  
684 inputs and continental weathering effects over the Cenozoic. *Earth and Planetary*  
685 *Science Letters*, **375**, 148–155.

- 686 Hein J. R., Koschinsky A., Bau M., Manheim F. T., Kand J. K. and Roberts L. (2000) Cobalt-  
687 rich ferromanganese crusts in the Pacific. In *Handbook of Marine Mineral Deposits*  
688 (ed. D. S. Cronan). CRC Press, London. pp. 239–278.
- 689 Heinrichs H., Schulz-Dobrick B., and Wedepohl K. H. (1980) Terrestrial geochemistry of Cd,  
690 Bi, Tl, Pb, Zn and Rb. *Geochimica et Cosmochimica Acta*, **44**, 1519–1533.
- 691 Huh Y., Chan L. H., Zhang L., and Edmond J. M. (1998) Lithium and its isotopes in major  
692 world rivers: implications for weathering and the oceanic budget. *Geochimica et*  
693 *Cosmochimica Acta*, **62**, 2039–2051.
- 694 Jacobson A. R., McBride M. B., Baveye P., and Steenhuis T. S. (2005) Environmental factors  
695 determining the trace-level sorption of silver and thallium to soils. *Science of the Total*  
696 *Environment*, **345**, 191–205.
- 697 Jay A. E. and Widdowson M. (2008) Stratigraphy, structure and volcanology of the SE  
698 Deccan continental flood basalt province: implications for eruptive extent and volumes.  
699 *Journal of the Geological Society of London*, **165**, 177–188.
- 700 Jones L. H. P. and Milne A. A. (1956) Birnessite, a New Manganese Oxide Mineral from  
701 Aberdeenshire, Scotland. *Mineralogical Magazine*, **31**, 283–288.
- 702 Kazantzis, G. (2000). Thallium in the environment and health effects. *Environmental*  
703 *Geochemistry and Health*, **22**, 275–280.
- 704 Kersten M., Xiao T., Kreissig K., Brett A., Coles B. J. and Rehkämper M. (2014) Tracing  
705 anthropogenic thallium in soil using stable isotope compositions. *Environmental*  
706 *Science & Technology*, **48**, 9030–9036.
- 707 Kisakürek B., Widdowson M. and James R. H. (2004) Behaviour of Li isotopes during  
708 continental weathering: The Bidar laterite profile, India. *Chemical Geology*, **212**, 27–  
709 44.
- 710 Klootwijk C.T. and Peirce J.W., 1979. India's and Australia's pole path since the late  
711 Mesozoic and the India–Asia collision. *Nature*, **282**, 605–607.
- 712 LaBrecque J. J. and Schorin H. (1987) Some statistical parameters for selected trace elements  
713 in VL-1. *Zeitschrift für Geomorphologie*, **64**, 33–38.
- 714 Law S., and Turner A. (2011) Thallium in the hydrosphere of south west England.  
715 *Environmental Pollution*, **159**, 3484 – 3489.
- 716 Liu S. A., Teng F. Z., Li S., Wei G. J., Ma J. L. and Li D. (2014) Copper and iron isotope  
717 fractionation during weathering and pedogenesis: Insights from saprolite profiles.  
718 *Geochimica et Cosmochimica Acta*, **146**, 59–75.
- 719 Ma J. L., Wei G. J., Xu Y. G., Long W. G. and Sun W. D. (2007) Mobilization and re-  
720 distribution of major and trace elements during extreme weathering of basalt in Hainan  
721 Island, South China. *Geochimica et Cosmochimica Acta*, **71**, 3223–3237.
- 722 Martini I. P. and Chesworth W. (1992) *Weathering, Soils and Paleosols*. Elsevier,  
723 Amsterdam, pp. 407–443.
- 724 Mason T. F. D. (1999) A combined chemical, mineralogical and isotopic study of lateritic  
725 soils from the Deccan Traps, S.W. India: implications for the processes which control  
726 laterite development. Master of Research Thesis, University of Edinburgh, U.K.
- 727 Nesbitt H. W. and Young G. M. (1989) Formation and diagenesis of weathering profiles.  
728 *Journal of Geology*, **97**, 129–147.
- 729 Nesbitt H. W., Markovics G., and Price R. G. (1980). Chemical processes affecting alkalis  
730 and alkaline earths during continental weathering. *Geochimica et Cosmochimica Acta*,  
731 **44**, 1659–1666.
- 732 Nielsen S. G., Rehkämper M., Baker J. and Halliday A. N. (2004) The precise and accurate  
733 determination of thallium isotope compositions and concentrations for water samples  
734 by MC-ICPMS. *Chemical Geology*, **204**, 109–124.

735 Nielsen S. G., Rehkämper M., Porcelli D., Andersson P., Halliday A. N., Swarzenski P. W.  
736 and Günther D. (2005) Thallium isotope composition of the upper continental crust and  
737 rivers - An investigation of the continental sources of dissolved marine thallium.  
738 *Geochimica et Cosmochimica Acta*, **69**, 2007–2019.

739 Nielsen S. G., Rehkämper M., Norman M. D., Halliday A. N. and Harrison D. (2006a)  
740 Thallium isotopic evidence for ferromanganese sediments in the mantle source of  
741 Hawaiian basalts. *Nature*, **439**, 314–317.

742 Nielsen S. G., Rehkämper M., Teagle D. A. H., Butterfield D. A., Alt J. C. and Halliday A.  
743 N. (2006b) Hydrothermal fluid fluxes calculated from the isotopic mass balance of  
744 thallium in the ocean crust. *Earth and Planetary Science Letters*, **251**, 120–133.

745 Nielsen S. G., Mar-Gerrison S., Gannoun A., LaRowe D., Klemm V., Halliday A. N. and  
746 Hein J. R. (2009) Thallium isotope evidence for a permanent increase in marine organic  
747 carbon export in the early Eocene. *Earth and Planetary Science Letters*, **278**, 297–307.

748 Nielsen S. G., Goff M., Hesselbo S. P., Jenkyns H. C., LaRowe D. E. and Lee C. T. A. (2011)  
749 Thallium isotopes in early diagenetic pyrite – A paleoredox proxy? *Geochimica et*  
750 *Cosmochimica Acta*, **75**, 6690–6704.

751 Nielsen S. G., Wasylenki L. E., Rehkämper M., Peacock C. L., Xue Z. and Moon E. M.  
752 (2013) Towards an understanding of thallium isotope fractionation during adsorption to  
753 manganese oxides. *Geochimica et Cosmochimica Acta*, **117**, 252–265.

754 Nielsen S. G., Yogodzinski G., Prytulak J., Plank T., Kay S. M., Kay R. W., Blusztajn J.,  
755 Owens, J. D., Auro M. and Kading T. (2016). Tracking along-arc sediment inputs to the  
756 Aleutian arc using thallium isotopes. *Geochimica et Cosmochimica Acta*, **181**, 217–  
757 237.

758 Nielsen S. G., Rehkämper M. and Prytulak J. (2017a) Investigation and application of  
759 thallium isotope fractionation. *Reviews in Mineralogy and Geochemistry*, **82**, 759–798.

760 Nielsen S. G., Prytulak J., Blusztajn J., Shu Y., Auro M., Regelous M. and Walker J. (2017b)  
761 Thallium isotopes as tracers of recycled materials in subduction zones: review and new  
762 data from Tonga-Kermadec and Central America. *Journal of Volcanology and*  
763 *Geothermal Research*, **339**, 23–40.

764 Pavlícková J., Zbírál J., Smatanová M., Habarta P., Houserová P. and Kubán V. (2006)  
765 Uptake of thallium from naturally-contaminated soils into vegetables. *Food Additives*  
766 *and Contaminants*, **23**, 484–91.

767 Peacock C. L., Moon E. M., Nielsen S. G. and Halliday A. N. (2009) Oxidative scavenging  
768 of Tl by Mn oxide birnessite: Sorption and stable isotope fractionation. *Goldschmidt*  
769 *Conference Proceedings Supplement 1*, A1003.

770 Peacock C. L. and Moon E. M. (2012) Oxidative scavenging of thallium by birnessite:  
771 Explanation for thallium enrichment and stable isotope fractionation in marine  
772 ferromanganese precipitates. *Geochimica et Cosmochimica Acta*, **84**, 297–313.

773 Poitrasson F., Viers J., Martin F. and Braun J.-J. (2008) Limited iron isotope variations in  
774 recent lateritic soils from Nsimi, Cameroon: implications for the global Fe geochemical  
775 cycle. *Chemical Geology*, **253**, 54–63.

776 Prinz, M. (1967). Geochemistry of basaltic rocks: trace elements. In: *Basalts* (Ed. Hess H. H.  
777 and Poldervaart A.). Interscience Publishers, p. 482

778 Prytulak J., Nielsen S. G., Plank T., Barker M. and Elliott T. (2013) Assessing the utility of  
779 thallium and thallium isotopes for tracing subduction zone inputs to the Mariana arc.  
780 *Chemical Geology*, **345**, 139–149.

781 Rehkämper M. and Halliday A. N. (1999) The precise measurement of Tl isotopic  
782 compositions by MC-ICPMS: Application to the analysis of geological materials and  
783 meteorites. *Geochimica et Cosmochimica Acta*, **63**, 935–944.

- 784 Rehkämper M., Frank M., Hein J. R., Porcelli D., Halliday A., Ingri J. and Liebetrau V.  
785 (2002) Thallium isotope variations in seawater and hydrogenetic, diagenetic, and  
786 hydrothermal ferromanganese deposits. *Earth and Planetary Science Letters*, **197**, 65–  
787 81.
- 788 Rehkämper M. and Nielsen S. G. (2004) The mass balance of dissolved thallium in the  
789 oceans. *Marine Chemistry*, **85**, 125–139.
- 790 Schauble E. A. (2007) Role of nuclear volume in driving equilibrium stable isotope  
791 fractionation of mercury, thallium, and other very heavy elements. *Geochimica et*  
792 *Cosmochimica Acta*, **71**, 2170–2189.
- 793 Schellmann W., (1986) A new definition of laterite. In *Lateritisation Processes. Memoirs of*  
794 *the Geological Survey of India 120* (ed. P. K. Banerji). Order of the Governor-General  
795 of India, India, pp. 1–7.
- 796 Schmidt P. W., Prasad V. and Ramam P. K. (1983) Magnetic ages of some Indian laterites.  
797 *Palaeogeography, Palaeoclimatology, Palaeoecology*, **44**, 185–202.
- 798 Schorin H. and LaBrecque J. J. (1983) A laterite standard reference material: Venezuelan  
799 Laterite VL-1. *Geostandards Newsletter*, **7**, 233–242.
- 800 Shaw D. M. (1952) The geochemistry of thallium. *Geochimica et Cosmochimica Acta*, **2**,  
801 118–154.
- 802 Tardy Y. (1997) *Petrology of Laterites and Tropical Soils*. A.A. Balkema, Rotterdam.
- 803 Taylor S. R., McLennan S. M. (1985) *The continental crust: its composition and evolution*.  
804 Blackwell Scientific Publication, Carlton.
- 805 Teng F.-Z., Watkins J. M., and Dauphas, N. (2017) Non-Traditional Stable Isotopes. *Reviews*  
806 *in Mineralogy & Geochemistry*, **82**.
- 807 Vaněk A., Chrastný V., Mihaljevič M., Drahota P., Grygar T. and Komárek M. (2009)  
808 Lithogenic thallium behavior in soils with different land use. *Journal of Geochemical*  
809 *Exploration*, **102**, 7–12.
- 810 Vaněk A., Komárek M., Vokurková P., Mihaljevič M., Šebek O., Panušková G. and Drábek  
811 O. (2011) Effect of illite and birnessite on thallium retention and bioavailability in  
812 contaminated soils. *Journal of Hazardous Materials*, **191**, 170–176.
- 813 Vaněk A., Grösslová Z., Mihaljevič M., Trubač J., Ettler V., Teper L., Cabala J., Rohovec J.,  
814 Zádorová T., Penížek V., Pavlů L., Holubík O., Němeček K., Houška J., Drábek O. and  
815 Ash C. (2016) Isotopic Tracing of Thallium Contamination in Soils Affected by  
816 Emissions from Coal-Fired Power Plants. *Environmental Science & Technology*, **50**,  
817 9864–9871.
- 818 Vaněk, A., Grösslová, Z., Mihaljevič, M., Ettler, V., Trubač, J., Chrastný, V., Penížek, V.,  
819 Teper, L., Cabala, J., Voegelin, A., Zádorová, T., Oborná, V., Drábek, O., Holubík, O.,  
820 Houška, J., Pavlů, L., and Ash, C. (2018). Thallium isotopes in metallurgical  
821 wastes/contaminated soils: A novel tool to trace metal source and behavior. *Journal of*  
822 *Hazardous Materials*, **343**, 78–85.
- 823 Voegelin A., Pfenninger N., Petrikis J., Majzlan J., Plötze M., Senn A. C., Mangold S.,  
824 Steininger R. and Göttlicher J. (2015) Thallium speciation and extractability in a  
825 thallium- and arsenic-rich soil developed from mineralized carbonate rock.  
826 *Environmental Science and Technology*, **49**, 5390–5398.
- 827 Wiederhold J. G. (2015) Metal stable isotope signatures as tracers in environmental  
828 geochemistry. *Environmental Science and Technology*, **49**, 2606–2624.
- 829 Widdowson M. (2007) Laterite and Ferricrete. In: *Geochemical Sediments and Landscapes*  
830 (eds. D. J Nash and S. J. McLaren). Wiley-Blackwell, Oxford, pp. 46–94.
- 831 Widdowson M. (2009) Evolution of Laterite in Goa. In: *Natural Resources of Goa: A*  
832 *Geological Perspective* (eds. A. Mascarenhas G. Kalavampara). Geological Survey of  
833 India, India, pp. 35–68.

- 834 Widdowson M. and Cox K. G. (1996) Uplift and erosional history of the Deccan traps, India:  
835 Evidence from laterites and drainage patterns of the Western Ghats and Konkan Coast.  
836 *Earth and Planetary Science Letters*, **137**, 57-69.
- 837 Widdowson M., and Gunnell Y. (1999a) Tertiary palaeosurfaces and lateritization of the  
838 coastal lowlands of Western Peninsula India. In *Palaeoweathering, Palaeosurfaces and*  
839 *Related Continental Deposits, Special Publication*. International Association of  
840 Sedimentologists, Gent. pp. 245-274.
- 841 Widdowson M. and Gunnell Y. (1999b) Lateritization, geomorphology and geodynamics of a  
842 passive continental margin: The Konkan and Kanara coastal lowlands of western  
843 Peninsular India. In: *Palaeoweathering, Palaeosurfaces and Related Continental*  
844 *Deposits. Special Publication 27, International Association of Sedimentologists* (eds.  
845 M. Thiry, R. Simon-Coinçon). Blackwell, Oxford, pp. 245–274.
- 846 Widdowson M. (1997). The geomorphological and geological importance of palaeosurfaces.  
847 *Geological Society, London, Special Publications*, **120**, 1–12.
- 848 Wimpenny J., Gannoun A., Burton K. W., Widdowson M., James R. H. and Gíslason S. R.  
849 (2007) Rhenium and osmium isotope and elemental behaviour accompanying laterite  
850 formation in the Deccan region of India. *Earth and Planetary Science Letters*, **261**,  
851 239–258.
- 852 Xiao T., Guha J., Boyle D., Liu C. Q., Zheng B., Wilson G. C. and Chen J. (2004) Naturally  
853 occurring thallium: A hidden geoenvironmental health hazard? *Environment*  
854 *International*, **30**, 501–507.

## 855 TABLES

856 Table 1 Thallium concentrations and  $\epsilon^{205}\text{Tl}$  from MC-ICPMS (Imperial College London) and ICP-MS (Open University) analyses of the basaltic BB and  
 857 greywacke SQ laterite sequences. A standard error of  $\pm 0.4 \epsilon^{205}\text{Tl}$  from long-term reproducibility is applied except in cases where this value is exceeded.

Sample	Depth (m)	Lithology	[Tl] ng/g MC-ICPMS	[Tl] ng/g ICP-MS	$\epsilon^{205}\text{Tl}$	2sd	# runs	# dissolutions
SQ2	34.0	Unweathered greywacke	559	540	-2.3	0.4	5	1
SQ3	30.0	Lighter greywacke	459	444	-1.3	0.5	1	1
SQ4	25.5	Soft weathered greywacke	231	218	-2.4	0.6	2	1
SQ5	22.5	Weathered greywacke	700	652	-2.1	0.6	4	2
SQ6	15.0	Red weathered greywacke	340	324	-1.9	0.5	1	1
SQ7	14.0	Base of laterite	148	126	-1.1	0.5	7	4
SQ8	13.5	Nodular laterite base	76	105	-0.5	0.4	2	1
SQ9	12.0	Nodular laterite	95	81	+0.3	0.4	2	1
SQ10	8.5	Semi-indurated laterite	40	37	-1.2	0.4	2	1
SQ11	7.5	Massive laterite	456	544	+3.5	0.6	2	1
SQ12	3.5	Indurated laterite cap	103	105	-1.0	0.4	2	1
SQ13	2.5	Indurated laterite cap	127	135	-1.0	0.4	4	1
BB5: Average	13.0	Basaltic saprolite	24	26	+6.2	1.5	4	3
BB5: Separate Runs								
BB5-1			27		+5.3			
BB5-2			25		+5.9			
BB5-2			25		+6.4			
BB5-3			28		+7.1			
BB7	6.0	Base of laterite	252	244	+0.3	0.5	1	1
BB8	5.0	Nodular laterite	38	39	-0.5	0.4	3	2



860 *Table 2 Thallium concentrations and  $\epsilon^{205}\text{Tl}$  of reference materials measured in this study from MC-ICPMS (Imperial College London) and ICP-MS (Open*  
 861 *University) analyses and from literature.*

Reference Materials		[Tl] ng/g MC-ICPMS	[Tl] ng/g ICP-MS	$\epsilon^{205}\text{Tl}$	2sd	# runs	# dissolutions
AGV-2, This study	Andesitic USGS standard	222		-2.6	0.6	10	4
AGV-2, Nielsen et al., 2017a	Andesitic USGS standard	269		-3.0	0.6	8	8
BCR-2, This study	Basaltic USGS standard	255		-2.5	0.4	4	2
BCR-2, Nielsen et al., 2017a	Basaltic USGS standard	257		-2.5	0.4	4	4
VL2	Venezuelan laterite standard	29	30	+2.1	0.5	2	2

	BB3	BB5	BB7	BB8	SQ1	SQ2	SQ3	SQ4	SQ5	SQ6	SQ7	SQ8	SQ9	SQ10	SQ11	SQ12	SQ13	SQ14	VL1	VL2
<b>Li</b>	6.8	3.7	11.2	17.4	7.4	31.6	32.4	12.5	45.0	20.2	13.8	9.7	8.7	4.5	4.2	7.1	9.5	8.8	0.1	2.8
<b>Sc</b>	68	77	34	47	43	12	13	7	11	10	15	16	17	24	27	28	38	66	64	82
<b>Ti</b>	26903	29298	16215	11650	8522	3243	3391	1809	2922	2563	4129	4558	3836	8646	2857	10307	8624	9471	16771	15681
<b>V</b>	730	1997	704	992	366	99	102	56	94	84	121	143	138	852	112	578	822	788	775	587
<b>Cr</b>	206	261	228	744	115	109	118	63	79	83	87	112	125	720	166	720	946	749	98	25
<b>Mn</b>	775	395	2401	464	1941	1031	831	508	1404	413	429	162	99	130	3720	344	256	245	494	730
<b>Co</b>	67	14	40	18	63	19	19	6	20	10	11	3	3	3	38	8	5	6	7	38
<b>Ni</b>	305	73	63	102	90	42	47	15	41	23	69	42	38	69	147	58	59	58	6	37
<b>Cu</b>	446	519	228	196	122	50	40	66	37	53	42	38	34	31	52	39	50	61	105	255
<b>Zn</b>	126	72	62	74	127	112	115	33	146	66	38	38	23	21	97	25	25	31	60	99
<b>Rb</b>	1.24	0.83	1.57	4.12	18.32	126.77	108.53	46.57	147.69	79.03	40.83	31.17	26.86	9.02	16.31	22.07	28.07	27.59	0.37	1.37
<b>Sr</b>	14	6	16	10	243	117	113	104	86	113	7	9	7	21	40	40	35	41	1	1
<b>Y</b>	796	14	6	8	31	17	27	13	17	40	12	9	8	10	27	17	14	19	3	7
<b>Zr</b>	253	315	193	224	66	172	192	83	137	123	213	196	191	203	76	261	217	236	421	419
<b>Nb</b>	19.6	25.5	15.2	17.0	3.3	13.8	15.0	7.1	12.5	10.8	16.8	17.6	16.0	20.8	8.1	32.9	27.3	30.7	17.2	18.2
<b>Sb</b>	0.09	0.31	0.81	1.41	0.02	0.24	0.34	0.24	0.30	0.26	0.41	0.62	0.60	11.53	1.12	8.40	14.46	8.30	0.74	0.31
<b>Cs</b>	0.112	0.101	0.140	0.403	0.556	4.314	3.538	1.284	4.506	2.104	1.107	1.502	0.896	0.441	1.704	1.323	1.920	1.595	0.011	0.092
<b>Ba</b>	57	16	445	18	144	702	609	404	665	549	571	473	454	46	730	136	136	125	6	32
<b>La</b>	33.3	9.6	28.7	13.3	8.2	25.7	41.9	15.1	13.4	72.1	7.3	6.9	3.4	19.6	54.0	40.6	29.4	32.1	2.1	4.4
<b>Ce</b>	25.9	22.5	270.1	27.6	20.4	52.8	75.5	32.7	27.8	98.9	63.4	21.2	9.1	33.5	87.9	87.3	63.1	60.1	14.7	164.4
<b>Pr</b>	16.78	4.07	3.97	2.61	2.85	5.62	7.88	3.50	2.96	12.38	1.99	1.64	0.81	2.97	8.49	6.33	4.90	5.66	0.47	1.29
<b>Nd</b>	77.3	18.2	11.9	9.5	13.7	20.1	28.1	12.7	10.7	43.4	7.6	6.0	3.1	9.4	26.5	20.1	16.0	19.4	1.8	5.4
<b>Sm</b>	29.70	4.49	2.01	1.98	3.85	3.72	5.06	2.51	2.14	7.91	1.58	1.18	0.68	1.55	4.93	3.23	2.78	3.51	0.53	1.59
<b>Eu</b>	12.27	1.11	0.51	0.48	1.41	0.82	0.96	0.57	0.54	1.62	0.40	0.31	0.22	0.31	1.14	0.58	0.53	0.67	0.15	0.42
<b>Gd</b>	56.98	3.62	2.64	1.72	4.28	3.02	4.41	2.27	1.98	7.45	1.53	1.02	0.64	1.33	5.11	2.64	2.29	2.87	0.51	1.91
<b>Tb</b>	12.85	0.63	0.28	0.30	0.77	0.46	0.67	0.36	0.33	1.14	0.25	0.18	0.13	0.22	0.82	0.40	0.37	0.46	0.11	0.27
<b>Dy</b>	93.32	3.65	1.50	1.85	4.93	2.67	3.95	2.18	2.13	6.36	1.74	1.29	1.00	1.47	4.94	2.53	2.31	3.06	0.73	1.69
<b>Ho</b>	24.79	0.76	0.32	0.42	1.11	0.59	0.87	0.46	0.53	1.28	0.42	0.33	0.27	0.35	1.07	0.61	0.53	0.67	0.18	0.38
<b>Er</b>	64.05	1.97	0.84	1.14	3.07	1.84	2.59	1.32	1.77	3.40	1.42	1.11	0.94	1.13	2.96	1.87	1.68	2.04	0.55	1.13
<b>Yb</b>	53.87	1.99	0.90	1.27	2.89	2.23	2.75	1.32	2.24	2.97	1.95	1.59	1.44	1.47	2.98	2.26	1.95	2.37	0.77	1.54
<b>Hf</b>	7.03	8.47	5.20	5.73	1.82	4.63	5.09	2.29	3.65	3.22	5.67	5.22	5.21	5.48	2.10	7.05	5.82	6.16	11.73	11.32
<b>Lu</b>	8.29	0.30	0.14	0.20	0.45	0.35	0.42	0.20	0.40	0.42	0.32	0.28	0.25	0.22	0.46	0.37	0.31	0.38	0.13	0.25
<b>Ta</b>	1.44	1.72	1.53	1.16	0.19	1.36	1.45	0.61	1.03	1.06	1.73	1.64	1.53	1.48	0.62	3.08	1.78	2.30	1.14	1.18
<b>Tl</b>	0.007	0.026	0.244	0.039	0.075	0.540	0.444	0.218	0.652	0.324	0.126	0.105	0.081	0.037	0.544	0.105	0.135	0.129	0.006	0.030
<b>Pb</b>	2.30	10.43	46.46	19.19	2.77	12.85	12.75	11.62	13.97	10.78	28.09	17.68	15.26	31.24	29.10	54.60	42.17	35.84	7.99	39.02
<b>Th</b>	1.92	3.60	3.82	10.06	0.47	21.06	21.51	7.61	15.51	13.63	26.82	21.94	23.64	20.80	6.06	24.91	22.02	22.61	14.00	11.02
<b>U</b>	1.01	2.19	1.24	2.00	0.09	5.90	6.32	2.19	4.81	4.07	6.29	5.81	6.21	4.52	6.79	6.65	7.39	10.37	1.69	3.14
<b>Sn</b>	1.85	0.53	0.79	1.09	0.75	3.11	2.34	1.71	3.84	1.98	3.25	3.20	3.09	2.61	1.45	5.46	2.69	3.01	2.47	0.46

Table 4  $\tau$ -values and Index of lateritization (IOL) values for BB and SQ profiles.

Sample	Depth (m)	$\tau$ -value	IOL	Degree of lateritization (Widdowson 2007)
<b>BB Sequence</b>				
BB9	2.0	20.1	90.1	Strongly lateritized
BB8	5.0	6.4	67.7	Moderately lateritized
BB7	6.0	52.8	61.7	Weakly lateritized
BB6*	11.0	2.9	93.8	Strongly lateritized
BB5	13.0	2.6	67.2	Allochthonous inputs
BB4*	15.0	1.8	58.0	Weakly lateritized
BB3	26.0	0.2	59.0	Weakly lateritized
BB2*	35.0	6.5	34.5	
BB1*	47.0		35.7	
	<b>Total</b>	93.2		
<b>SQ Sequence</b>				
SQ14	0.0	-0.8	85.8	Strongly lateritized
SQ13	2.5	-0.8	82.0	Strongly lateritized
SQ12	3.5	-0.9	79.8	Moderately lateritized
SQ11	7.5	1.3	84.3	Strongly lateritized
SQ10	8.5	-0.9	82.3	Strongly lateritized
SQ9	12.0	-0.9	30.5	Kaolinized
SQ8	13.5	-0.8	30.7	Kaolinized
SQ7	14.0	-0.8	26.9	Kaolinized
SQ6	15.0	-0.2	18.3	
SQ5	22.5	0.5	27.2	Kaolinized
SQ4	25.5	-0.2	14.8	
SQ3	30.0	-0.3	21.9	
SQ2	34.0		23.4	
	<b>Total</b>	-4.8		

$\tau$ - values calculated following Chadwick et al. (1990). The BB sequence is calculated relative to BB1 protolith values from Babechuk et al., 2014 (Supplementary Sheet 1). The Index of Lateritization is calculated following Schellman (1986), using major oxide wt% values from Widdowson (2007) alongside degrees of lateritization determined by Widdowson (2007) from ternary plots.

868 **FIGURE CAPTIONS**

869 Figure 1: Literature compilation of Tl concentrations and Tl stable isotopes ( $\epsilon^{205}\text{Tl}$ ) for  
870 terrestrial and major marine sediments and reservoirs. (a – d) FeMn deposits (Rehkämper et  
871 al., 2002), (e) mantle (Nielsen et al., 2006b), (f) low temperature altered ocean crust (Nielsen  
872 et al., 2006a), (g – j) volcanoclastics/radiolarian and claystone/pelagic clays (Prytulak et al.,  
873 2013 and Nielsen et al., 2017b), (j) diatom-bearing sediments (Nielsen et al., 2016), (k – l)  
874 river water and loess averages (Nielsen et al., 2005), (m) continental crust average (Nielsen et  
875 al., 2017a), (n) soils (Kersten et al., 2014), and laterite values measured in this study. Where  
876 average ranges specified  $\epsilon^{205}\text{Tl} \pm 1\text{SD}$  are reported.

877

878 Figure 2: Inset showing the study region and map of the location of the two laterite  
879 sequences (adapted from Wimpenny et al., 2007).

880

881 Figure 3: Schematic profiles of the laterite sequences at a) Goa (SQ) and b) Bidar (BB),  
882 alongside alteration zones (adapted from Wimpenny et al., 2007). Zone I = unaltered to  
883 weakly altered substrate, II = saprolite, III = palaeowater table and IV = Fe-rich lateritic cap,  
884 as noted by Widdowson (2007). Samples analysed in this study for trace element  
885 concentrations highlighted in colour and for Tl stable isotopes denoted by an \*. Values for  
886  $\text{K}_2\text{O}$ ,  $\text{MnO}$  and  $\text{MgO}$  content plotted on log axes. Measured values denoted by filled symbols  
887 and literature values by unfilled symbols throughout (Widdowson, 2007).

888

889 Figure 4: (a) Thallium concentration versus depth-for the SQ greywacke (orange  
890 throughout) and BB basalt (blue throughout) – based laterites. (b) Thallium stable isotope  
891 variations with depth for the greywacke and basalt. The deepest basaltic sample at 47 m  
892 (BB1) is an estimated unaltered basaltic or mantle composition (Nielsen et al., 2017a).

893

894 Figure 5: Trace element data for alkali elements, alkaline earths and Tl for the a) SQ  
895 profile, measured in this study using ICP-QQQ. and b) BB profile, with both measured and  
896 literature values. Alkali elements and alkaline earth elements plotted on log scale and where  
897 used, literature values are denoted by unfilled symbols (see Supplementary Sheet 1;  
898 Widdowson, 2007 and Wimpenny et al., 2007).

899

900 Figure 6: Thallium concentrations and  $\epsilon^{205}\text{Tl}$  variations for the greywacke (orange) and  
901 basalt (blue). BB5 and SQ11 display heavy positive excursions. Literature values for BB1  
902 denoted by unfilled triangle (Nielsen et al., 2017a).

903

904 Figure 7:  $\tau_{\text{Tl/Zr}}$  variations with depth through the (a) SQ profile and (b) BB profile. Both  
905 profiles show contrasting behaviours in net trends but horizons with distinct Tl addition are  
906 present in both. For the BB profile literature values for Tl and Zr concentrations are denoted  
907 by unfilled symbols (see Supplementary Sheet 1, Widdowson (2007)).

908

909 Figure 8: The effect of increasing intensity of lateritization on Tl concentration. Zones are  
910 labelled, with Zone I = unaltered to weakly altered substrate, II = saprolite, III = palaeowater  
911 table and IV = Fe-rich lateritic cap throughout.

912

913 Figure 9: The role of increasing weathering intensity, as quantified by the index of  
914 lateritization, on Tl stable isotopes across the SQ profile. Correlation is shown for samples  
915 not weathered beyond the stage of kaolinization (Widdowson, 2007).

916

917 Figure 10: Trends within the SQ profile between  $\epsilon^{205}\text{Tl}$  and  $\tau_{\text{Tl/Zr}}$  through the full profile  
918 (a) are masked by the large excursive palaeowater table horizon (SQ11, Zone III). Further  
919 analysis discounting SQ11 show a weak negative correlation between Tl stable isotope  
920 composition and Tl enrichments.

921

922 Figure 11: The effect of weathering on  $\tau_{\text{Tl/Zr}}$  (as a measure of Tl mobility within the SQ  
923 profile).

924

## 925 **SUPPLEMENTARY MATERIAL**

926 Supplementary Sheet 1: Major elemental literature compilation from Widdowson, 2007.

927 Supplementary Sheet 2: Trace elemental literature compilation from Widdowson, 2007  
928 and Babechuk et al., 2014.

929 Supplementary Sheet 3: Trace element data quality control.

930 Supplementary Sheet 4: Trace elemental data from ICP-QQQ.

931 Electronic Annex: Comparison of methods for determination of thallium Tl concentration  
932 using ICP-MS (Open University) and MC ICP-MS (Imperial College London).

933

## 1 TABLES

2 *Table 1 Thallium concentrations and  $\epsilon^{205}\text{Tl}$  from MC-ICPMS (Imperial College London) and ICP-MS (Open University) analyses of the basaltic BB and*  
 3 *greywacke SQ laterite sequences. A standard error of  $\pm 0.4 \epsilon^{205}\text{Tl}$  from long-term reproducibility is applied except in cases where this value is exceeded.*

Sample	Depth (m)	Lithology	[Tl] ng/g MC-ICPMS	[Tl] ng/g ICP-MS	$\epsilon^{205}\text{Tl}$	2sd	# runs	# dissolutions
SQ2	34.0	Unweathered greywacke	559	540	-2.3	0.4	5	1
SQ3	30.0	Lighter greywacke	459	444	-1.3	0.5	1	1
SQ4	25.5	Soft weathered greywacke	231	218	-2.4	0.6	2	1
SQ5	22.5	Weathered greywacke	700	652	-2.1	0.6	4	2
SQ6	15.0	Red weathered greywacke	340	324	-1.9	0.5	1	1
SQ7	14.0	Base of laterite	148	126	-1.1	0.5	7	4
SQ8	13.5	Nodular laterite base	76	105	-0.5	0.4	2	1
SQ9	12.0	Nodular laterite	95	81	+0.3	0.4	2	1
SQ10	8.5	Semi-indurated laterite	40	37	-1.2	0.4	2	1
SQ11	7.5	Massive laterite	456	544	+3.5	0.6	2	1
SQ12	3.5	Indurated laterite cap	103	105	-1.0	0.4	2	1
SQ13	2.5	Indurated laterite cap	127	135	-1.0	0.4	4	1
BB5: Average	13.0	Basaltic saprolite	24	26	+6.2	1.5	4	3
BB5: Separate Runs								
BB5-1			27		+5.3			
BB5-2			25		+5.9			
BB5-2			25		+6.4			
BB5-3			28		+7.1			
BB7	6.0	Base of laterite	252	244	+0.3	0.5	1	1
BB8	5.0	Nodular laterite	38	39	-0.5	0.4	3	2

6 *Table 2 Thallium concentrations and  $\epsilon^{205}\text{Tl}$  of reference materials measured in this study from MC-ICPMS (Imperial College London) and ICP-MS (Open*  
 7 *University) analyses and from literature.*

8

Reference Materials		[Tl] ng/g MC-ICPMS	[Tl] ng/g ICP-MS	$\epsilon^{205}\text{Tl}$	2sd	# runs	# dissolutions
AGV-2, This study	Andesitic USGS standard	222		-2.6	0.6	10	4
AGV-2, Nielsen et al., 2017a	Andesitic USGS standard	269		-3.0	0.6	8	8
BCR-2, This study	Basaltic USGS standard	255		-2.5	0.4	4	2
BCR-2, Nielsen et al., 2017a	Basaltic USGS standard	257		-2.5	0.4	4	4
VL2	Venezuelan laterite standard	29	30	+2.1	0.5	2	2



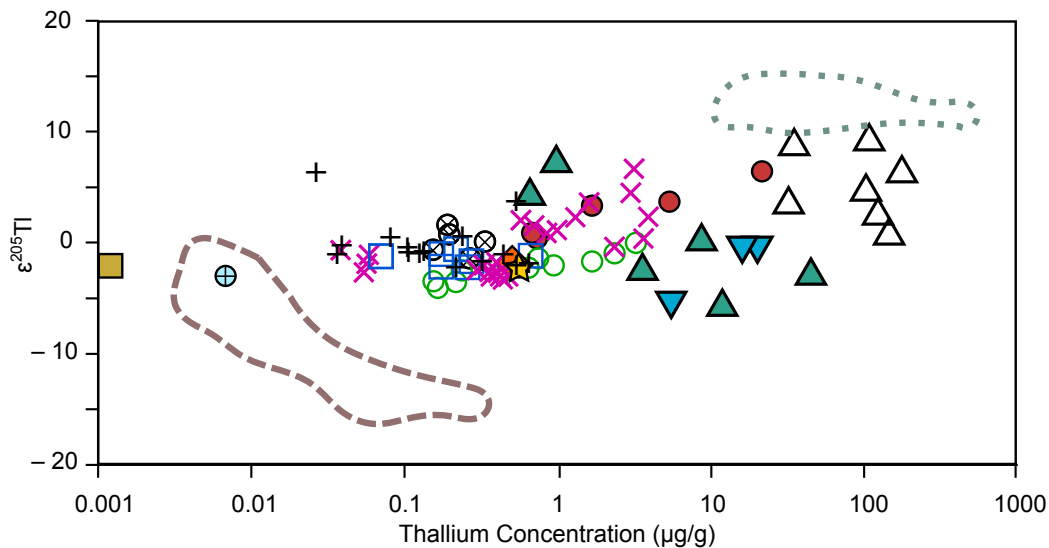
Table 3 Trace element concentrations determined by ICP-MS at the Open University ( $\mu\text{g/g}$ ).

	BB3	BB5	BB7	BB8	SQ1	SQ2	SQ3	SQ4	SQ5	SQ6	SQ7	SQ8	SQ9	SQ10	SQ11	SQ12	SQ13	SQ14	VL1	VL2
<b>Li</b>	6.8	3.7	11.2	17.4	7.4	31.6	32.4	12.5	45.0	20.2	13.8	9.7	8.7	4.5	4.2	7.1	9.5	8.8	0.1	2.8
<b>Sc</b>	68	77	34	47	43	12	13	7	11	10	15	16	17	24	27	28	38	66	64	82
<b>Ti</b>	26903	29298	16215	11650	8522	3243	3391	1809	2922	2563	4129	4558	3836	8646	2857	10307	8624	9471	16771	15681
<b>V</b>	730	1997	704	992	366	99	102	56	94	84	121	143	138	852	112	578	822	788	775	587
<b>Cr</b>	206	261	228	744	115	109	118	63	79	83	87	112	125	720	166	720	946	749	98	25
<b>Mn</b>	775	395	2401	464	1941	1031	831	508	1404	413	429	162	99	130	3720	344	256	245	494	730
<b>Co</b>	67	14	40	18	63	19	19	6	20	10	11	3	3	3	38	8	5	6	7	38
<b>Ni</b>	305	73	63	102	90	42	47	15	41	23	69	42	38	69	147	58	59	58	6	37
<b>Cu</b>	446	519	228	196	122	50	40	66	37	53	42	38	34	31	52	39	50	61	105	255
<b>Zn</b>	126	72	62	74	127	112	115	33	146	66	38	38	23	21	97	25	25	31	60	99
<b>Rb</b>	1.24	0.83	1.57	4.12	18.32	126.77	108.53	46.57	147.69	79.03	40.83	31.17	26.86	9.02	16.31	22.07	28.07	27.59	0.37	1.37
<b>Sr</b>	14	6	16	10	243	117	113	104	86	113	7	9	7	21	40	40	35	41	1	1
<b>Y</b>	796	14	6	8	31	17	27	13	17	40	12	9	8	10	27	17	14	19	3	7
<b>Zr</b>	253	315	193	224	66	172	192	83	137	123	213	196	191	203	76	261	217	236	421	419
<b>Nb</b>	19.6	25.5	15.2	17.0	3.3	13.8	15.0	7.1	12.5	10.8	16.8	17.6	16.0	20.8	8.1	32.9	27.3	30.7	17.2	18.2
<b>Sb</b>	0.09	0.31	0.81	1.41	0.02	0.24	0.34	0.24	0.30	0.26	0.41	0.62	0.60	11.53	1.12	8.40	14.46	8.30	0.74	0.31
<b>Cs</b>	0.112	0.101	0.140	0.403	0.556	4.314	3.538	1.284	4.506	2.104	1.107	1.502	0.896	0.441	1.704	1.323	1.920	1.595	0.011	0.092
<b>Ba</b>	57	16	445	18	144	702	609	404	665	549	571	473	454	46	730	136	136	125	6	32
<b>La</b>	33.3	9.6	28.7	13.3	8.2	25.7	41.9	15.1	13.4	72.1	7.3	6.9	3.4	19.6	54.0	40.6	29.4	32.1	2.1	4.4
<b>Ce</b>	25.9	22.5	270.1	27.6	20.4	52.8	75.5	32.7	27.8	98.9	63.4	21.2	9.1	33.5	87.9	87.3	63.1	60.1	14.7	164.4
<b>Pr</b>	16.78	4.07	3.97	2.61	2.85	5.62	7.88	3.50	2.96	12.38	1.99	1.64	0.81	2.97	8.49	6.33	4.90	5.66	0.47	1.29
<b>Nd</b>	77.3	18.2	11.9	9.5	13.7	20.1	28.1	12.7	10.7	43.4	7.6	6.0	3.1	9.4	26.5	20.1	16.0	19.4	1.8	5.4
<b>Sm</b>	29.70	4.49	2.01	1.98	3.85	3.72	5.06	2.51	2.14	7.91	1.58	1.18	0.68	1.55	4.93	3.23	2.78	3.51	0.53	1.59
<b>Eu</b>	12.27	1.11	0.51	0.48	1.41	0.82	0.96	0.57	0.54	1.62	0.40	0.31	0.22	0.31	1.14	0.58	0.53	0.67	0.15	0.42
<b>Gd</b>	56.98	3.62	2.64	1.72	4.28	3.02	4.41	2.27	1.98	7.45	1.53	1.02	0.64	1.33	5.11	2.64	2.29	2.87	0.51	1.91
<b>Tb</b>	12.85	0.63	0.28	0.30	0.77	0.46	0.67	0.36	0.33	1.14	0.25	0.18	0.13	0.22	0.82	0.40	0.37	0.46	0.11	0.27
<b>Dy</b>	93.32	3.65	1.50	1.85	4.93	2.67	3.95	2.18	2.13	6.36	1.74	1.29	1.00	1.47	4.94	2.53	2.31	3.06	0.73	1.69
<b>Ho</b>	24.79	0.76	0.32	0.42	1.11	0.59	0.87	0.46	0.53	1.28	0.42	0.33	0.27	0.35	1.07	0.61	0.53	0.67	0.18	0.38
<b>Er</b>	64.05	1.97	0.84	1.14	3.07	1.84	2.59	1.32	1.77	3.40	1.42	1.11	0.94	1.13	2.96	1.87	1.68	2.04	0.55	1.13
<b>Yb</b>	53.87	1.99	0.90	1.27	2.89	2.23	2.75	1.32	2.24	2.97	1.95	1.59	1.44	1.47	2.98	2.26	1.95	2.37	0.77	1.54
<b>Hf</b>	7.03	8.47	5.20	5.73	1.82	4.63	5.09	2.29	3.65	3.22	5.67	5.22	5.21	5.48	2.10	7.05	5.82	6.16	11.73	11.32
<b>Lu</b>	8.29	0.30	0.14	0.20	0.45	0.35	0.42	0.20	0.40	0.42	0.32	0.28	0.25	0.22	0.46	0.37	0.31	0.38	0.13	0.25
<b>Ta</b>	1.44	1.72	1.53	1.16	0.19	1.36	1.45	0.61	1.03	1.06	1.73	1.64	1.53	1.48	0.62	3.08	1.78	2.30	1.14	1.18
<b>Tl</b>	0.007	0.026	0.244	0.039	0.075	0.540	0.444	0.218	0.652	0.324	0.126	0.105	0.081	0.037	0.544	0.105	0.135	0.129	0.006	0.030
<b>Pb</b>	2.30	10.43	46.46	19.19	2.77	12.85	12.75	11.62	13.97	10.78	28.09	17.68	15.26	31.24	29.10	54.60	42.17	35.84	7.99	39.02
<b>Th</b>	1.92	3.60	3.82	10.06	0.47	21.06	21.51	7.61	15.51	13.63	26.82	21.94	23.64	20.80	6.06	24.91	22.02	22.61	14.00	11.02
<b>U</b>	1.01	2.19	1.24	2.00	0.09	5.90	6.32	2.19	4.81	4.07	6.29	5.81	6.21	4.52	6.79	6.65	7.39	10.37	1.69	3.14
<b>Sn</b>	1.85	0.53	0.79	1.09	0.75	3.11	2.34	1.71	3.84	1.98	3.25	3.20	3.09	2.61	1.45	5.46	2.69	3.01	2.47	0.46

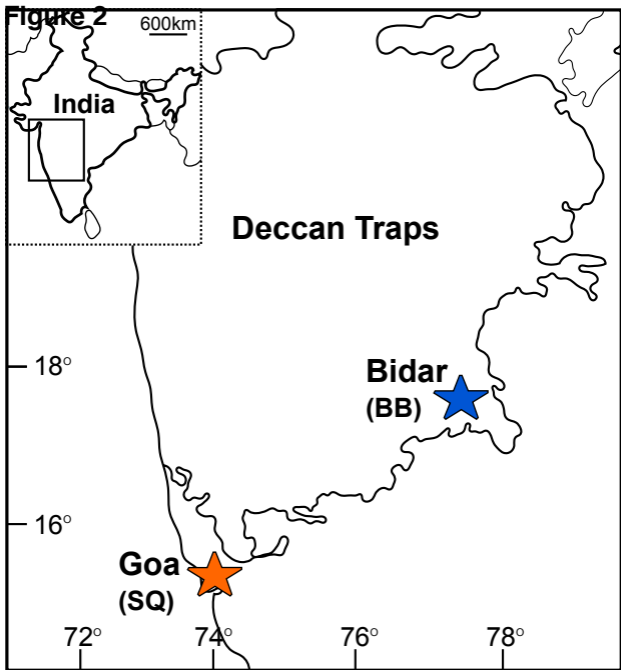
Table 4  $\tau$ -values and Index of lateritization (IOL) values for BB and SQ profiles.

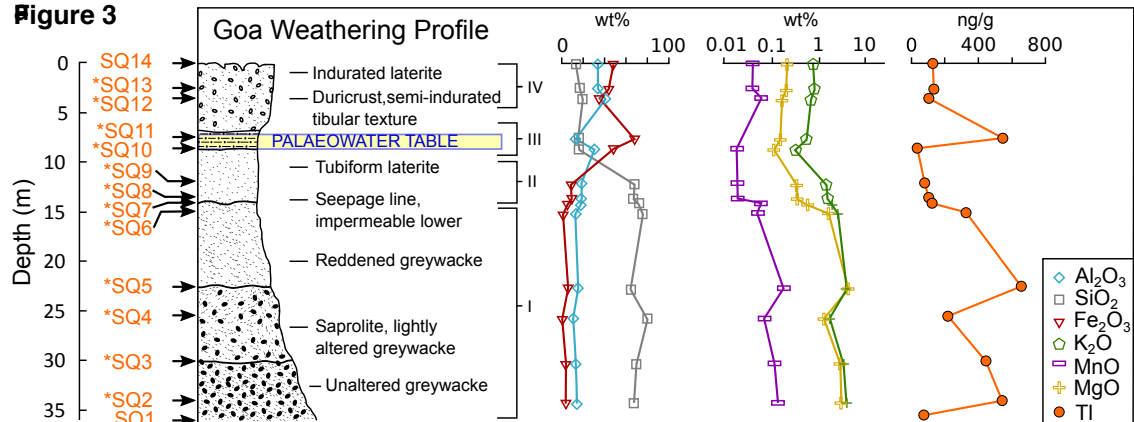
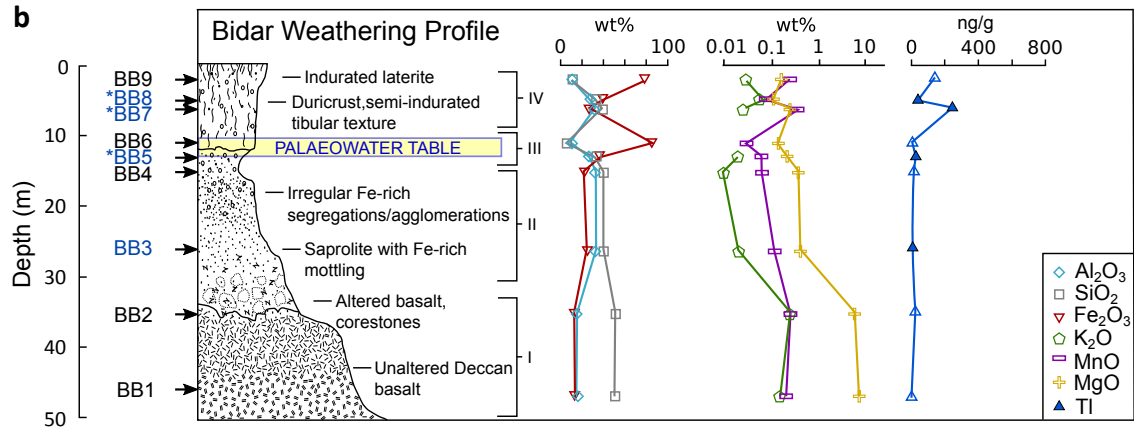
Sample	Depth (m)	$\tau$ -value	IOL	Degree of lateritization (Widdowson 2007)
<b>BB Sequence</b>				
BB9	2.0	20.1	90.1	Strongly lateritized
BB8	5.0	6.4	67.7	Moderately lateritized
BB7	6.0	52.8	61.7	Weakly lateritized
BB6*	11.0	2.9	93.8	Strongly lateritized
BB5	13.0	2.6	67.2	Allochthonous inputs
BB4*	15.0	1.8	58.0	Weakly lateritized
BB3	26.0	0.2	59.0	Weakly lateritized
BB2*	35.0	6.5	34.5	
BB1*	47.0		35.7	
		<b>Total</b>	93.2	
<b>SQ Sequence</b>				
SQ14	0.0	-0.8	85.8	Strongly lateritized
SQ13	2.5	-0.8	82.0	Strongly lateritized
SQ12	3.5	-0.9	79.8	Moderately lateritized
SQ11	7.5	1.3	84.3	Strongly lateritized
SQ10	8.5	-0.9	82.3	Strongly lateritized
SQ9	12.0	-0.9	30.5	Kaolinized
SQ8	13.5	-0.8	30.7	Kaolinized
SQ7	14.0	-0.8	26.9	Kaolinized
SQ6	15.0	-0.2	18.3	
SQ5	22.5	0.5	27.2	Kaolinized
SQ4	25.5	-0.2	14.8	
SQ3	30.0	-0.3	21.9	
SQ2	34.0		23.4	
		<b>Total</b>	-4.8	

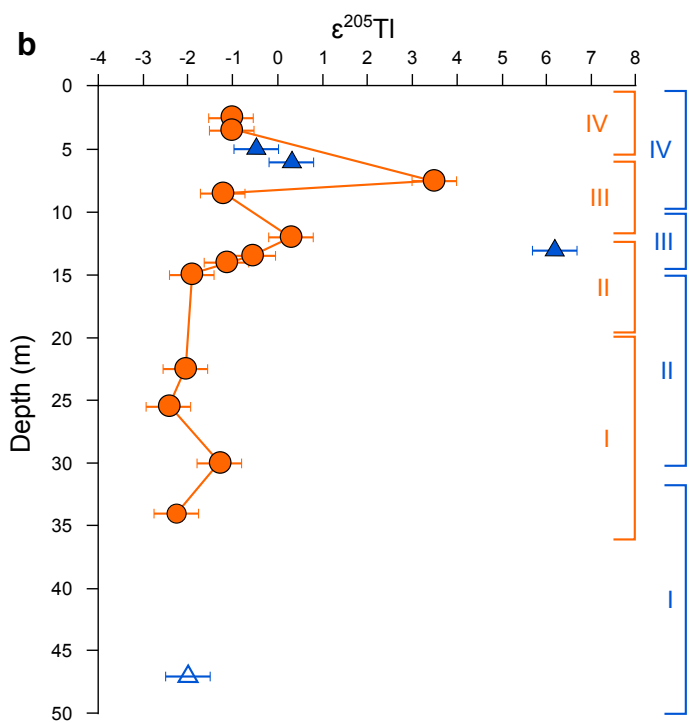
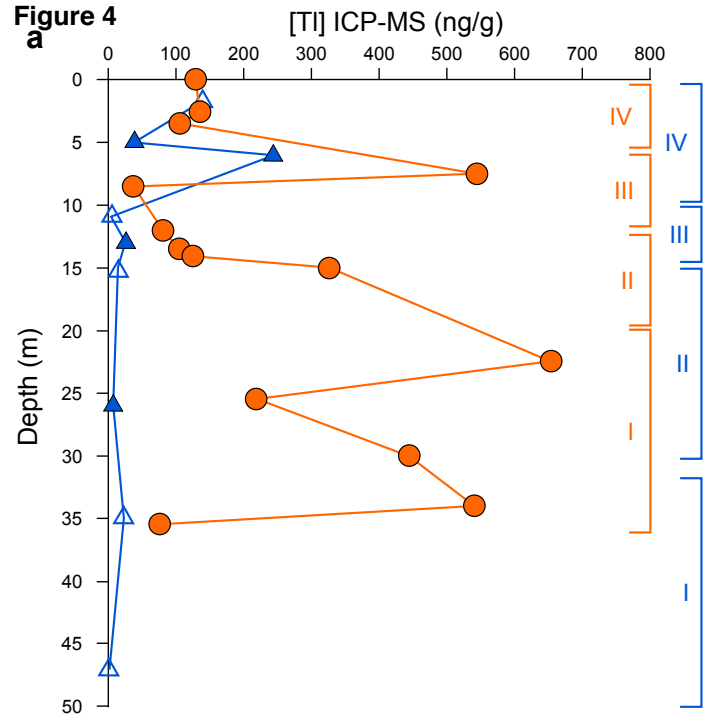
$\tau$ - values calculated following Chadwick et al. (1990). The BB sequence is calculated relative to BB1 protolith values from Babechuk et al., 2014 (Supplementary Sheet 1). The Index of Lateritization is calculated following Schellman (1986), using major oxide wt% values from Widdowson (2007) alongside degrees of lateritization determined by Widdowson (2007) from ternary plots.

**Figure 1**

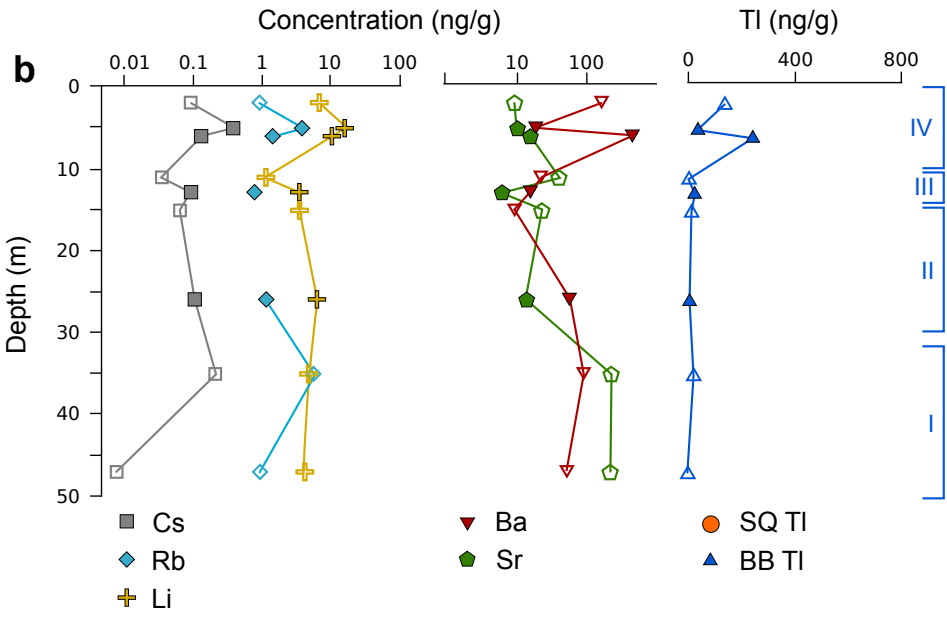
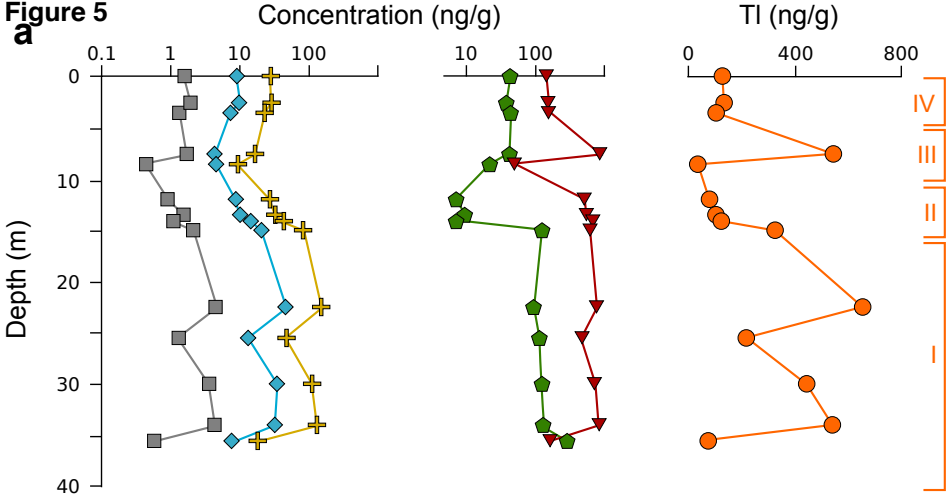
- Hydrogenetic FeMn deposits<sup>(a)</sup>
- ▲ Hydrothermal FeMn deposits<sup>(b)</sup>
- ▼ Shallow water diagenetic FeMn deposits<sup>(c)</sup>
- △ Deep water diagenetic FeMn deposits<sup>(d)</sup>
- Mantle<sup>(e)</sup>
- Low-T altered oceanic crust<sup>(f)</sup>
- Red-brown clays<sup>(g)</sup>
- × Pelagic clays and silts<sup>(h)</sup>
- ⊗ Volcaniclastics<sup>(i)</sup>
- Diatom-bearing sediments<sup>(j)</sup>
- ⊕ River water average  $\pm 1.9$ <sup>(k)</sup>
- ★ Loess average  $\pm 0.3$ <sup>(l)</sup>
- ◆ Continental crust average  $\pm 1$ <sup>(m)</sup>
- Soils<sup>(n)</sup>
- ⊕ Laterites (this study)



**Figure 3****b**

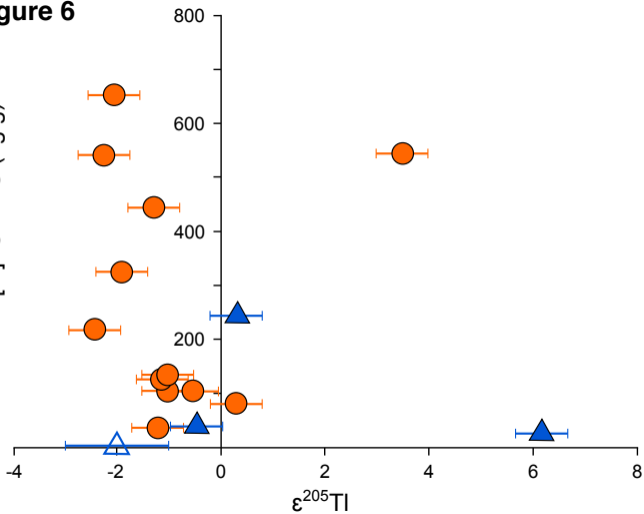
**Figure 4**

**Figure 5**

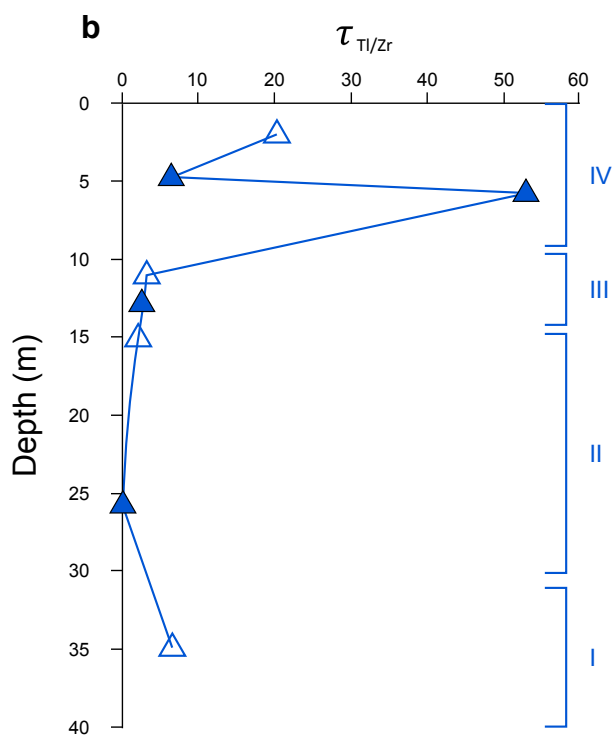
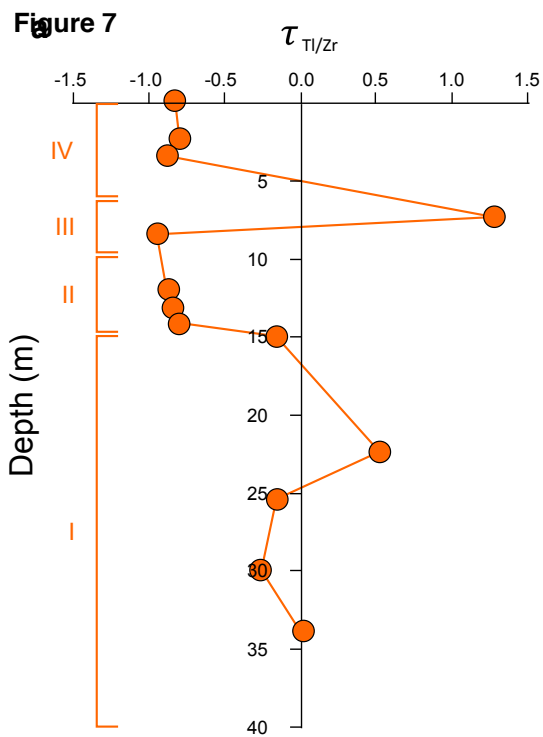


**Figure 6**

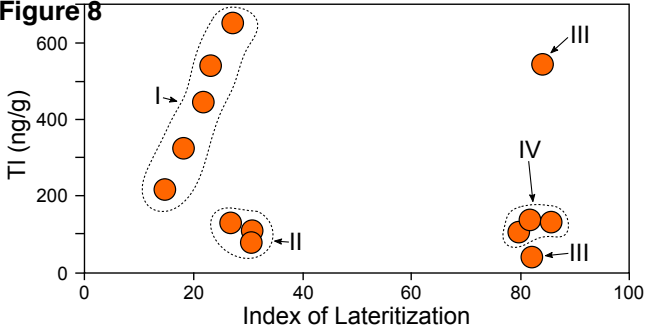
[Tl] ICP-MS (ng/g)



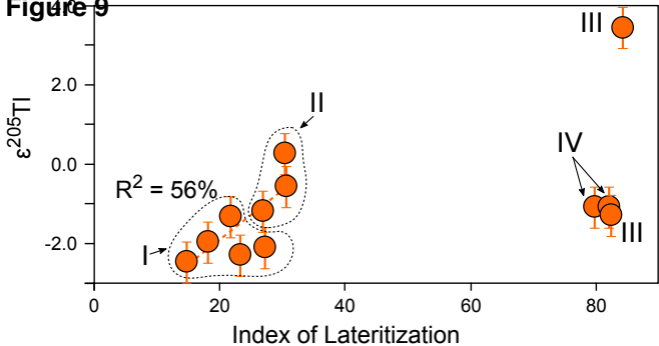


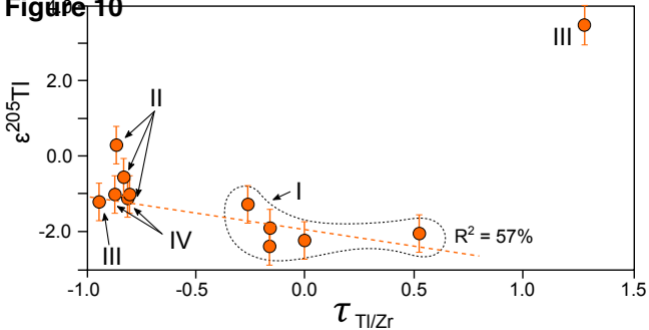


**Figure 8**

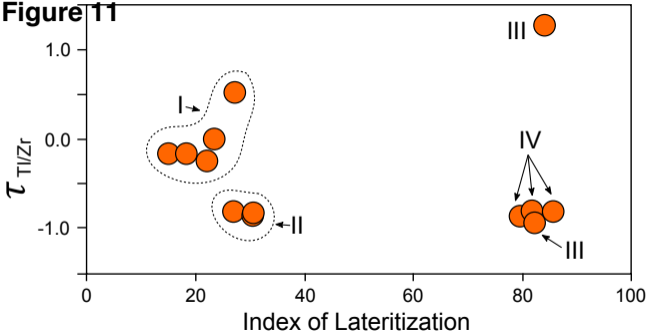


**Figure 9**



**Figure 10**

**Figure 11**



**Supplementary Sheet**

[Click here to download Appendix: Supplementary Sheet.xls](#)

## Formulae

[Click here to download Appendix: FORMULAE.pdf](#)

**Electronic Annex Figure**

[Click here to download Electronic Annex: ElectronicAnnexFigure.pdf](#)